Geophys. J. Int. (2007) **168,** 843–862 doi: 10.1111/j.1365-246X.2006.03201.x

Effects of elasticity on the Rayleigh–Taylor instability: implications for large-scale geodynamics

Boris J. P. Kaus and Thorsten W. Becker

Department of Earth Sciences, University of Southern California, 3651 *Trousdale Parkway, Los Angeles,* CA-90089-740, *USA.*
E-mail: bkaus@usc.edu

Accepted 2006 August 22. Received 2006 August 15; in original form 2006 February 22

SUMMARY

Although parts of the lithosphere may be expected to behave elastically over certain timescales, this effect is commonly ignored in models of large-scale mantle dynamics. Recently it has been demonstrated that elasticity, and in particular viscoelasticity, may have a significant effect on the buckling instability and on the creation of lithospheric-scale shearzones. It is, however, less clear whether elasticity also has an effect on mantle convection and density-driven lithospheric instabilities. The focus of this work is, therefore, to study the effects of elasticity on the two-layer Rayleigh–Taylor (RT) instability, consisting of a Maxwell viscoelastic layer overlying a viscous layer of lower density. We analyse this problem by performing systematic numerical simulations that are compared with newly derived analytical solutions. It is demonstrated that elasticity can be important for certain parameter combinations; it leads to a speedup of the RT instability. The cause for this speedup is that the RT instability is only sensitive to the viscous fraction of deformation in the viscoelastic layer. Elasticity reduces the viscous fraction of deformation at timescales shorter than the Maxwell relaxation time t_M($t_M = \mu/G$, where μ is the viscosity and G the elastic shear module). For plate tectonics on Earth, the parameters are such that the effect of elasticity on instability growth is negligible for most boundary conditions. Whereas elasticity does not (or only slightly) change the timescales for lithospheric detachment of the upper mantle, it does significantly alter the response and stress build-up in the overlying crust. Numerical simulations illustrate this effect for lithospheric detachment and show that peak stresses in a viscoelastic crust are smaller than stresses that develop in a viscous crust. Moreover, if the timescale for delamination of the mantle lithosphere is equal or smaller than the Maxwell relaxation time of the crust, the topography of the crust is increased compared to viscous models.

Key words: elasticity, gravitational instability, lithospheric dynamics, mantle lithosphere, Rayleigh–Taylor instability.

1 INTRODUCTION

There is little discussion about the fact that rocks behave elastically at short timescales but may flow in a ductile manner over longer periods of time. Evidence for this comes, for example, from seismic waves, post-glacial and post-seismic rebound studies and plate bending under seamounts. Yet it is not entirely clear what the role of elasticity is in large-scale geodynamic processes. Part of the problem seems to be technical; only over the last decade or so have new numerical techniques been developed that include both the effects of elasticity as well as large-strain, incompressible viscous flow (Melosh 1978; Poliakov *et al.* 1993; Braun & Sambridge 1994; Batt & Braun 1997; Toth & Gurnis 1998; Frederiksen & Braun 2001; Schmalholz *et al.* 2001; Vasilyev *et al.* 2001; Moresi *et al.* 2002, 2003; Kaus *et al.* 2004; Kaus 2005; Mühlhaus & Regenauer-Lieb 2005). Another part of the problem is that the few studies that do include elastic effects typically also include additional complexities such as brittle failure. Whereas a visco-elasto-plastic rheology is certainly more applicable to the lithosphere than merely viscoelastic rheologies, it is difficult to isolate viscoelastic effects from previous model results. Moreover, most studies are purely numerical in nature and are rarely backed up with analytical solutions. The consequence is that there is currently little understanding (and agreement) on how (and if) the presence of elasticity changes the dynamics of processes such as mantle convection. Our goal is, therefore, to study the effects of elasticity (or viscoelasticity) in a simplified, but well defined, model of density-driven flow. Our numerical results are compared with analytical work and give insight in how elasticity changes the mechanics of these instabilities. This is useful in interpreting more realistic models, and to estimate the importance of elasticity for geodynamic settings.

Early numerical modelling studies of thermal convection with Maxwellian fluids (Ivins *et al.* 1982; Harder 1991) demonstrated that convection is more vigorous when elastic effects are important. These studies treated the viscosity of the mantle as being constant, which is a possible explanation for the fact that numerical problems limited solutions to small Deborah numbers. More recent studies, incorporating the effects of temperature-dependent viscosity, suggest that elasticity may have the effect to cause slab roll-back (Moresi *et al.* 2002) and decrease dissipation in subducting slabs (Mühlhaus & Regenauer-Lieb 2005). Models that study subduction processes (Gurnis *et al.* 1996; Funiciello *et al.* 2003) concluded that whereas forebulges can be created by viscous flow only (Gurnis *et al.* 1996), model fits improve if elasticity is included (Funiciello *et al.* 2003; Hall & Gurnis 2005). Similar conclusions have been obtained for barythmetic profiles at mid-oceanic ridges (Bercovici *et al.* 1992).

Initiation of subduction is another process that appears to be facilitated by the effects of elasticity (Toth & Gurnis 1998; Regenauer-Lieb *et al.* 2001; Hall *et al.* 2003). In most models, subduction initiation is preceded by shear localization due to weakening of either cohesion and friction angle (Hall *et al.* 2003) or of effective viscosity (Regenauer-Lieb *et al.* 2001). Elasticity is helpful in these cases since it releases non-dissipative, elastically stored energy in small zones, which may result in strong weakening (Ogawa 1987; Regenauer-Lieb *et al.* 2001; Kaus 2005; Kaus & Podladchikov 2006), sometimes accompanied with thermal runaway processes (Ogawa 1987; Kaus & Podladchikov 2006).

Models of plume–lithosphere interaction show that elastic bending stresses are non-negligible in a viscoelastic lithosphere which causes stresses in the order of a few hundreds MPa (Podladchikov *et al.* 1993; Vasilyev *et al.* 2001; Burov & Guillou-Frottier 2005). A number of studies concentrated on the buckling of highly viscous and viscoelastic layers embedded in a viscous matrix (Schmalholz & Podladchikov 1999, 2001; Schmalholz *et al.* 2002, 2005). This instability is relevant for both outcrop-scale structures such as folds and for lithospheric-scale deformation (Burg & Podladchikov 1999; Gerbault 2000; Toussaint *et al.* 2004). Elastic effects significantly increase dominant growth rates as well as alter dominant wavelengths of the buckling instability compared to the viscous end-member models.

Finally, the effects of elasticity on the Rayleigh–Taylor (RT) instability have been studied in a number of analytical and numerical models (Biot 1965; Biot & Odé 1965; Odé 1966; Naimark & Ismail-Zadeh 1994; Poliakov *et al.* 1993). Most of these studies concluded that elasticity facilitates the growth of the RT instability. However, they have either been restricted to a limited set of boundary conditions, or to isoviscous systems. It is thus worthwhile to further evaluate the relevance of elastic effects for geodynamic processes.

2 RHEOLOGY

To review some basic findings of viscoelastic analysis, we first consider a zero-dimensional example. For a constant strain rate $\dot{\varepsilon}^{\mathrm{vis}}$, a Newtonian viscous body will develop a stress τ, given by (Ranalli 1995; Schubert *et al.* 2001)

$$\tau = 2\mu\dot{\varepsilon}^{\mathrm{vis}}, \tag{1}$$

where μ is the shear viscosity of the material. Viscous dissipation is constant.

Deviatoric stress in a purely elastic body, on the other hand, is related to the absolute strain. Under the small-strain assumption, the deviatoric stressing rate is related to the applied background strain rate $\dot{\varepsilon}^{\mathrm{el}}$ as

$$\frac{\partial \tau}{\partial t} = 2G\dot{\varepsilon}^{\mathrm{el}}, \tag{2}$$

where t is time and G the elastic shear modulus. Stress evolution can be obtained by integrating eq. (2), which yields $\tau(t) = \tau(0) + 2G\dot{\varepsilon}^{\mathrm{el}}t$, where $\tau(0)$ is the initial stress. Elastic strain energy increases with ongoing deformation.

A Maxwell viscoelastic body (an elastic and viscous body connected in series) is the simplest rheological material that fits observed post-glacial rebound data (Peltier 1985). The relationship between deviatoric strain rate and stress is in this case given by

$$\frac{1}{2G}\frac{\partial \tau}{\partial t} + \frac{1}{2\mu}\tau = \dot{\varepsilon} = \dot{\varepsilon}^{\mathrm{el}} + \dot{\varepsilon}^{\mathrm{vis}}. \tag{3}$$

Under a constant background applied strain rate, $\dot{\varepsilon}_0$, eq. (3) can be solved for τ by integrating over time:

$$\tau(t) = 2\mu\left(1 - e^{-t/t_M}\right)\dot{\varepsilon}_0 + \tau(0)e^{-t/t_M}, \tag{4}$$

where $t_M = \mu/G$ is the Maxwell relaxation time. From eq. (4) we can compute an apparent viscosity μ_{app} as

$$\mu_{\mathrm{app}} = \frac{\tau(t)}{2\dot{\varepsilon}_0} = \mu - \left(\mu - \mu_{\mathrm{app}}(0)\right)e^{-t/t_M}, \tag{5}$$

with $\mu_{\mathrm{app}}(0) = \tau(0)/(2\dot{\varepsilon}_0)$. Viscoelasticity thus results in a time-dependent viscosity (Fig. 1). In the case that the initial stress $\tau(0)$ is lower than the steady-state viscous stress $2\mu\dot{\varepsilon}_0$, μ_{app} is lower than μ for $\sim$3 Maxwell times (Fig. 1).

An interesting question is how much of the deformation is taken up by elastic and viscous deformation. Their respective fractions (f_{el} and f_{vis}) can be computed from eq. (3) as

$$1 = \frac{\dot{\varepsilon}^{\mathrm{el}}}{\dot{\varepsilon}_0} + \frac{\dot{\varepsilon}^{\mathrm{vis}}}{\dot{\varepsilon}_0} = f_{\mathrm{el}} + f_{\mathrm{vis}}. \tag{6}$$

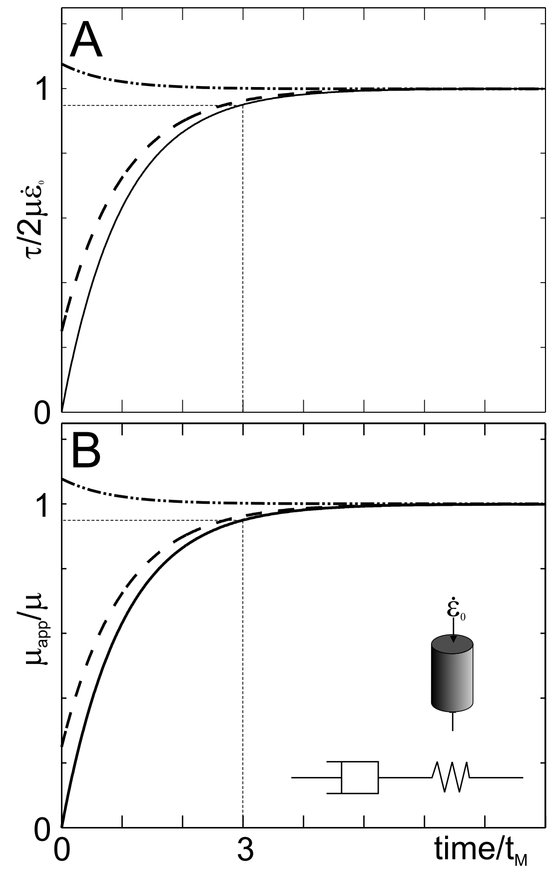

Figure 1. (a) Non-dimensional deviatoric stress versus non-dimensional time under a constant applied background strain rate for a Maxwell viscoelastic rheology. Results are shown for two different values of initial stress. (b) Normalized apparent viscosity versus time for the same simulations as in (a). Apparent viscosity increases with time until it reaches the 'true' viscosity if the initial stress is smaller than the steady-state viscous stress.

An explicit relationship for f_{vis} is then given by

$$f_{\mathrm{vis}} = \frac{\tau(t)}{2\mu\dot{\varepsilon}_0}$$
$$f_{\mathrm{vis}} = \frac{\mu_{\mathrm{app}}}{\mu} = 1 - \left(1 - \frac{\tau(0)}{2\mu\dot{\varepsilon}_0}\right) e^{-t/t_M}. \tag{7}$$

The elastic part of the deformation is given by $f_{\mathrm{el}} = 1 - f_{\mathrm{vis}}$. Thus, in a case with $\tau(0) = 0$, the initial response is fully elastic ($f_{\mathrm{vis}} = 0$), whereas it is fully viscous ($f_{\mathrm{vis}} = 1$) at $t \gg t_M$. The apparent viscosity is a proxy for the viscous fraction of the deformation (eq. 7). We show below that the viscoelastic RT instability is sensitive to the viscous fraction of the deformation only. An important consequence of this is that viscoelastic instabilities may be faster than their respective viscous counterparts (at least if $\tau(0) < 2\mu\dot{\varepsilon}_0$, so that $f_{\mathrm{vis}}(0) < 1$).

In the Earth, the elastic shear module is relatively well-constrained, ($G \simeq 10^{10}$–10^{11} Pa for the lithosphere, for example, from PREM; Dziewonski & Anderson (1981)). The effective viscosity, however, is highly variable. Allowing effective viscosity values of $\mu = 10^{17}$–10^{27} Pa s yields Maxwell relaxation times between 11 days and 3.2 Byrs. Processes that take place on timescales that are significantly shorter than t_M may be influenced by the effects of elasticity.

3 MODEL

Rocks are compressible if deformed elastically but nearly incompressible in a viscous deformation mode (Schubert *et al.* 2001). In most of this work we assume, for reasons of simplicity, that rocks are incompressible. We performed a range of numerical experiments to address this approximation. The results indicate that the effects of elastic bulk compressibility on the growth of the RT instability are small, in agreement with earlier work on the viscoelastic folding (Mancktelow 2001) and the RT instability (Poliakov *et al.* 1993). In two dimensions, we can then write

$$\frac{\partial v_i}{\partial x_i} = 0, \tag{8}$$

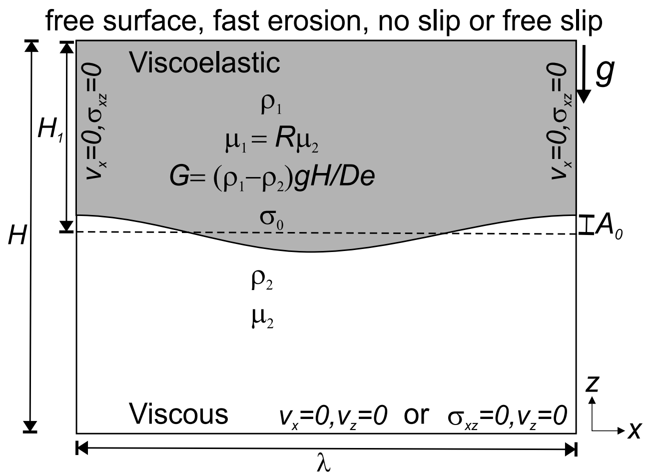

Figure 2. Model set-up employed in this work. The side boundary conditions are free slip (or periodic in the semi-analytical solution), the lower boundary condition is free slip or no-slip and a range of upper boundary conditions are employed (see Appendix A for a more detailed explanation of the upper boundary conditions).

where v_i is velocity, x_i are spatial coordinates, $i = 1, 2$, and the Einstein summation convection applies. Assuming that the effects of inertia can be ignored, force equilibrium gives

$$\frac{\partial \sigma_{ij}}{\partial x_j} = \rho g_i, \tag{9}$$

where σ_{ij} are stresses, ρ is density and $g_i = (0, g)$ is the gravitational acceleration in z-direction. We define

$$\sigma_{ij} = -P\delta_{ij} + \tau_{ij}, \tag{10}$$

where τ_{ij} are deviatoric stresses, δ_{ij} the Kronecker delta and pressure P is given by $P = -\frac{\sigma_{ii}}{2}$. The (deviatoric) strain rate is defined in the usual way, $\dot{\varepsilon}_{ij} = \frac{1}{2}(\frac{\partial v_i}{\partial x_j} + \frac{\partial v_j}{\partial x_i})$, and the rheology is Maxwell viscoelastic, leading to a multidimensional version of eq. (3)

$$\dot{\varepsilon}_{ij} = \dot{\varepsilon}_{ij}^{\mathrm{vis}} + \dot{\varepsilon}_{ij}^{\mathrm{el}} = \frac{1}{2\mu}\tau_{ij} + \frac{1}{2G}\frac{D\tau_{ij}}{Dt}, \tag{11}$$

where D/Dt denotes the objective derivative of the stress tensor versus time t. We employ the Jaumann objective formulation, which is given by:

$$\frac{D\tau_{ij}}{Dt} = \frac{\partial \tau_{ij}}{\partial t} + \underbrace{v_k \frac{\partial \tau_{ij}}{\partial x_k}}_{\text{advection}} \underbrace{-W_{ik}\tau_{kj} + \tau_{ik}W_{kj}}_{\text{rotation}}, \tag{12}$$

where $W_{ij} = \frac{1}{2}(\frac{\partial v_i}{\partial x_j} - \frac{\partial v_j}{\partial x_i})$ is the vorticity. Mühlhaus & Regenauer-Lieb (2005) show that rotational terms are only important for unrealistically large values of stress (see also Kaus 2005). For the sake of completeness, however, we employ the full objective stress derivative in the numerical code. In deriving the analytical solutions, both advection and rotation terms are ignored.

3.1 Non-dimensionalization

Our model consists of a viscoelastic layer of thickness H_1, with density ρ_1, viscosity μ_1 and elastic shear module G_1 that overlies a viscous layer of thickness $H - H_1$, with density ρ_2 and viscosity μ_2 (Fig. 2). The interface between the two fluids is perturbed sinusoidally according to $h(x) = (H - H_1) + A_0 \cos(2\pi/\lambda x)$, where H_1 is the thickness of the upper layer, H the height of the model, A_0 the initial amplitude and λ the wavelength of the perturbation. If $\rho_1 > \rho_2$, the system is gravitationally unstable.

The number of non-dimensional parameters that arise can be minimized by choosing $\sigma^* = (\rho_1 - \rho_2)gH$, $t^* = \mu_2/((\rho_1 - \rho_2)gH)$, and $L^* = H$ as characteristic values for stress, time and length, respectively. The constitutive law (eq. 11) in non-dimensional form (with˜denoting non-dimensional variables) is then

$$-De\frac{D\tilde{\tau}_{ij}}{D\tilde{t}} + 2\tilde{\dot{\varepsilon}}_{ij} = \tilde{\tau}_{ij}. \tag{13}$$

Here,

$$De = \frac{(\rho_1 - \rho_2)gH}{G}, \tag{14}$$

is the Deborah number, which is here defined as the ratio between the viscous (Stokes) timescale $(= (\rho_1 - \rho_2)gH/\mu_1)$ and the viscoelastic timescale $(= \mu_1/G)$ of the upper layer (Poliakov *et al.* 1993). Interestingly, the Deborah number, which is a measure of the importance of elasticity (compare eqs 1 and 13), is independent on the viscosity of the system. This is due to the fact that the magnitude of stress is solely dependent on the density difference for purely buoyancy-driven flow. The dynamics of the viscoelastic RT instability thus differs significantly from that of other instabilities such as buckling (Schmalholz & Podladchikov 1999). There, the characteristic stress is given by the viscous background stress, which depends on the background strain rate and the effective viscosity of the system.

In the present definition of the Deborah number realistic values for lithospheric-scale deformation are $10^{-4} \leq De \leq 1$ (with $\Delta\rho =$ 10–330 kg m^{-3}, $g = 10$ ms^{-2}, $H = 100$–3000 km, $G = 10^{10}$–10^{11} Pa). Systems with $De = O(1)$ may result in unrealistically large buoyancy stresses, once perturbations reach amplitudes of $\sim O(H)$. In reality such stresses cannot exist, since they exceed the theoretical yield strength of materials ($\sim$0.1 G). Thus other deformation mechanisms, such as plastic failure, will take over before such stresses will be reached. At smaller values of stress (for smaller amplitudes), the mechanical behaviour of the system is viscoelastic, however, and our definition of the Deborah number characterizes the effective mechanical response of the system.

Another parameter controlling the dynamics of the system is the viscosity contrast between the upper and the lower layer, expressed by

$$R = \frac{\mu_1}{\mu_2}. \tag{15}$$

For a lithosphere–mantle system, typically $R > 1$. The thickness of the upper, high-viscosity, layer is given by H_1, and the thickness ratio by:

$$T = \frac{H_1}{H}. \tag{16}$$

If a free-surface upper boundary condition is present, the additional parameter

$$D_{\mathrm{surf}} = \frac{\rho_1 - \rho_2}{\rho_1 - \rho_{\mathrm{air}}}, \tag{17}$$

expresses the normalized density difference between air and rocks. For geophysically relevant cases, $\rho_{\mathrm{air}} \approx 0$ and $D_{\mathrm{surf}} < 0.2$ (Poliakov & Podladchikov 1992).

Viscoelastic rheology is sensitive to the initial stress. We have employed two techniques to set the initial stress in the viscoelastic layer. For the first, we compute the stress distribution for given initial conditions assuming a purely viscous rheology for the upper layer. This gravity-driven stress is multiplied with a factor B_{fac} and the result is employed as initial stress of the model. The second technique assumes that initial, far-field pure-shear, extension or compression was present before the onset of gravity-driven deformation. The magnitude of this stress can be measured by

$$B_{\mathrm{vis}} = \frac{\sigma_0}{(\rho_1 - \rho_2) g H}, \tag{18}$$

where σ_0 is the initial pre-stress. The vertical deviatoric stress τ_{zz} is used as a measure of the initial stress ($\sigma_0 = \tau_{zz}$). B_{vis} thus indicates the magnitude of the initial over the maximum density-driven viscous stress. Positive and negative B_{vis} numbers indicate an initial compressive and extensional stress, respectively.

In our model, five non-dimensional parameters (De, R, $B_{\mathrm{vis}}/B_{\mathrm{fac}}$, D_{surf} and T) govern the dynamics. Compared to viscous models, viscoelasticity introduces two new parameters, $B_{\mathrm{vis}}/B_{\mathrm{fac}}$ and De. Poliakov *et al.* (1993) studied the effect of De on the growth rate of the RT instability. They demonstrated that the effect of elasticity is to enhance the growth rate of the instability. However, their analysis was restricted to $B_{\mathrm{vis}} = 0$, a fixed wavelength and viscosity contrast and to free-slip boundary conditions. Here we extend their study by including a wider range of boundary conditions and by studying the effect of changing R and $B_{\mathrm{vis}}/B_{\mathrm{fac}}$.

4 SEMI-ANALYTICAL METHOD

Perturbation analysis of the RT instability states that the growth in amplitude versus time of a sinusoidal perturbation is exponential

$$A(t) = A_0 e^{qt}, \tag{19}$$

where A_0 is the initial amplitude, and q the growth rate. This growth rate depends on material parameters such as viscosity contrast, boundary conditions and geometrical constraints. In the general non-Newtonian viscous case, closed form analytical expressions for q can be derived for a two-layer system (Biot & Odé 1965; Fletcher 1972; Fletcher & Hallet 1983; Ricard & Froidevaux 1986; Zuber *et al.* 1986; Bassi & Bonnin 1988; Conrad & Molnar 1997; Burg *et al.* 2004), with free-slip, no-slip or fast erosion upper boundary conditions. Viscous rheologies are characterized by a direct proportionality between strain rate and deviatoric stress. In the viscoelastic case, such a proportionality is no longer given; instead, stress is time dependent, which allows the derivation of simple analytical solutions only for very specific, and restricted, cases (one such case is addressed below). For the more general case, we have derived a set of (non-linear) ordinary differential equations, which can be solved numerically to yield a semi-analytical solution. These new solutions are in good agreement with our numerical results, as we show below.

A proxy for the velocity of the sinusoidally perturbed interface of amplitude A, and thus the strain rate in the model, is given by

$$\frac{\partial A}{\partial t} = q_{\mathrm{eff}} A, \tag{20}$$

and

$$\dot{\varepsilon} = \frac{1}{H}\frac{\partial A}{\partial t}. \tag{21}$$

The stress evolution is given by the general Maxwell relationship (eq. 11). Ignoring advective and rotational terms, this yields

$$\frac{\partial \tau}{\partial t} = 2G\dot{\varepsilon} - \frac{G}{\mu}\tau. \tag{22}$$

The viscous fraction of the deformation is given by

$$f_{\mathrm{vis}} = \frac{\dot{\varepsilon}^{\mathrm{vis}}}{\dot{\varepsilon}} = \frac{\tau H}{2\mu \frac{\partial A}{\partial t}}. \tag{23}$$

The main assumption in our model is that in a viscoelastic layer only the viscous fraction f_{vis} of the deformation contributes to the growth of the RT instability. The growth rate q_{eff} can than be computed from the classical viscous analysis if the apparent viscosity, $\mu_{\mathrm{app}} = f_{\mathrm{vis}}\,\mu$, rather than μ is used as a proxy for the viscosity of the viscoelastic layer. In our model set-up (Fig. 2), only the upper layer is viscoelastic. Thus the growth rate q_{eff} is computed from the viscous growth rate q as

$$q_{\mathrm{eff}} = q\left(f_{\mathrm{vis}}\frac{\mu_1}{\mu_2}, T, \lambda, \Delta\rho, BC's\right). \tag{24}$$

The viscous growth rate can be taken from literature or can be derived for a specific case. Appendix A gives a brief outline of the procedure used in this work.

The equations that govern model behaviour in our two-layer model can thus be summarized as

$$\begin{aligned} \frac{\partial A}{\partial t} &= q_{\mathrm{eff}} A \\ \frac{\partial \tau}{\partial t} &= \frac{2G}{H}\frac{\partial A}{\partial t} - \frac{G}{\mu_1}\tau \\ q_{\mathrm{eff}} &= q\left(\frac{\tau H}{2\mu \frac{\partial A}{\partial t}}\frac{\mu_1}{\mu_2}, T, \lambda, \Delta\rho, BC's\right). \end{aligned} \tag{25}$$

As initial conditions, we employ

$$A(0) = A_0$$

and

$$\tau(0) = 2\mu_1 \frac{q\left(\frac{\mu_1}{\mu_2}, T, \lambda, \Delta\rho, BC's\right) A_0}{H} B_{\mathrm{fac}}.$$

The initial condition for stress is a proxy for the viscous stress with an initial amplitude A_0, multiplied by a factor B_{fac}.

Eqs (25) with initial conditions (26) have been numerically integrated forwards in time, using an adaptive time step, implicit ODE solver. Iterations are employed at every time step to treat the non-linearities that arise from the dependence of q_{eff} on strain rate and stress.

5 NUMERICAL METHOD

Analytical and semi-analytical solutions are only valid for small amplitudes. Moreover, we make many simplifying assumptions such as ignoring advection and rotation of stress. It is thus important to compare the analytical results with a numerical technique which can correctly integrate the governing equations up to finite amplitudes. For this purpose, we use a recently developed 2-D numerical code, SloMo, that uses the finite element technique to solve the governing equations for slowly moving viscoelastoplastic materials (Kaus 2005; Buiter *et al.* 2006). The velocity–pressure formulation is employed with admissible Crouzeix–Raviart $Q_2 - P_1$ quadrilateral elements (Cuvelier *et al.* 1986). A newly introduced feature of the code is the ability to treat both compressible and incompressible materials in the same computational domain. In the case of incompressible flow, we employ Uzawa iterations to enforce incompressibility (Poliakov & Podladchikov 1992; Cuvelier *et al.* 1986).

Here, we are mainly interested in how the initial growth rate of the RT instability changes as a function of elastic parameters. It is, therefore, desirable to have a solution as accurate as possible during these stages. Typically, Eulerian-based flow solvers that incorporate the effects of viscoelasticity suffer from numerical issues such as diffusion of stresses, or oscillations of stresses due to out-of-balance interpolated stresses. Whereas Lagrangian codes suffer from the same issues whenever remeshing is applied, these issues do not arise until the remeshing stage. For these reasons, we used the code in a purely Lagrangian manner and determined growth rates before remeshing was employed. The code has been extensively benchmarked versus analytical solutions for the RT and the folding instability as well as for various 0-D rheological models (see Kaus 2005; Kaus & Schmalholz 2006, for different benchmark comparisons)). The incorporation of elastic bulk compressibility in the code was verified with an analytical solution for self-compaction of viscoelastic materials under the influence of gravity and with a 0-D extension/compression test for which a simple solution can be derived (results available upon request).

The gravity-driven initial stress state is numerically obtained by computing the stress from a purely viscous model, which is then multiplied with a factor B_{fac}. The pure-shear initial stress state is computed by imposing a pure-shear background deformation to the model. The background strain rate $\dot{\varepsilon}_{BG}$ is chosen such that $\tau_{zz} = \sigma_0 = 2\mu_1\dot{\varepsilon}_{BG}$, $\tau_{xx} = -\sigma_0$, far away from the perturbed interface. Both methods result in an initial stress state that is in force balance.

6 RESULTS

In the first part of this section we analyse the effects of elasticity on the RT instability by deriving an analytical solution for the case of a viscoelastic layer on top of an infinite viscous half-space. Then we employ both semi-analytical and numerical methods to study the more general case in which

(1) the lower layer is allowed to have a finite thickness,
(2) the upper boundary condition is varied and
(3) the effect of non-zero initial stress is taken into account.

Finally, we show results from a few, more realistic, numerical models that address the gravitational instability of the mantle lithosphere.

6.1 Analytical solution for a viscoelastic layer overlying an infinite viscous half-space

A closed-form analytical solution for the viscoelastic RT instability can be derived only in a number of, somewhat restricted, cases. One such case is a system in which a viscoelastic lithosphere of thickness H_1 and with viscosity μ_1 and elastic shear module G overlies an infinite viscous half-space of viscosity μ_2. The viscous growth rate, q, is in this case given by

$$q = \frac{\Delta\rho g H_1}{\mu_2}\frac{(1+R)\,e^{2k} + (-1+R)\,e^{-2k} - 2\,R - 4\,k}{k\,((2\,R + R^2 + 1)\,e^{2k} + (2\,R - R^2 - 1)\,e^{-2k} + 4\,R^2 k - 4\,k)}, \tag{26}$$

where $k = \frac{2\pi}{\lambda}$ is the wavenumber, and we assume free-slip upper boundary conditions. For a given wavelength of $\lambda/H_1 \le 4$ a numerical approximation of this equation is given by

$$q \approx \frac{\Delta\rho g H_1}{\mu_2}\frac{c}{1+R}, \tag{27}$$

where c is a wavelength-dependent constant given by $c \approx 0.07957, 0.15493, 0.2295$ for $\lambda/H_1 = 1$, 2 and 4, respectively (the maximum relative error of this approximation varies from ~1 per cent for $\lambda/H_1 = 1$ to ~18 per cent for $\lambda/H_1 = 4$). The governing equations in dimensional form are then (*cf.* eqs 25):

$$\begin{aligned} \dot{A} &= \frac{\Delta\rho g H_1}{\mu_2}\frac{c}{1 + \frac{H_1 \tau}{2\mu_1 A}\frac{\mu_1}{\mu_2}} A \\ \dot{\tau} &= \frac{2G}{H_1}\dot{A} - \frac{G}{\mu_1}\tau, \end{aligned} \tag{28}$$

with $\dot{A} = \frac{\partial A}{\partial t}$, $\dot{\tau} = \frac{\partial \tau}{\partial t}$. In addition we assume $A(0) = A_0$ and $\tau'(0) = 2\,cA_0\,RB_{\mathrm{fac}}/(1+R)$. If we choose H_1, $\Delta\rho g H_1$ and $\mu_2/(\Delta\rho g H_1)$ as characteristic scales for length, stress and time, respectively, the equations can be written in non-dimensional form as

$$\begin{aligned} \dot{A}' &= \frac{c}{\left(1 + \frac{\tau'}{2A'}\right)} A' \\ \tau' &= 2R\dot{A}' - De_1 R\dot{\tau}', \end{aligned} \tag{29}$$

where $De_1 = \frac{\Delta\rho g H_1}{G}$ is the Deborah number of this set-up and $'$ indicates non-dimensional parameters. From this representation, it can be observed that the limiting case of $De_1 \to 0$ yields the viscous case. An analytical solution of eqs (29) can be found, and the solution for $A'(t')$ is given by

$$A'(t') = \frac{A_0}{2}\left(e^{at'} + e^{bt'} - \frac{\left(-1 - De_1\,Rc - R^2 - 2R + (-1 + 2\,B_{\mathrm{fac}})\,De_1\,R^2 c\right)\left(e^{at'} - e^{bt'}\right)}{\sqrt{K}\,(1+R)}\right), \tag{30}$$

where

$$\begin{aligned} a &= \frac{-R - 1 + cDe_1\,R + \sqrt{K}}{2De_1\,R} \\ b &= \frac{-R - 1 + cDe_1\,R - \sqrt{K}}{2De_1\,R} \\ K &= R^2 + 2R - 2\,cDe_1\,R^2 + 1 + 2\,cDe_1\,R + c^2 {De_1}^2 R^2. \end{aligned}$$

A plot of $A'(t')$ versus t' for the case of a highly viscous viscoelastic layer overlying an infinite viscous mantle with $B_{\mathrm{fac}} = 0$ (Fig. 3a) reveals that elasticity generally enhances the growth of the RT instability. A small parameter range exists in eq. (30) during which elasticity slows down the growth of the RT instability for a finite period of time (if $B_{\mathrm{fac}} > 1$). At even larger values of B_{fac}, however, negative amplitudes develop which we consider unphysical.

The time it takes a viscous instability to grow from its initial amplitude until an amplitude $A' = 1$ is for the present set-up given by

$$t_v = -\frac{\log(A_0)(1+R)}{c}. \tag{31}$$

A more systematic analysis can be made by defining the time, t_{ve}, it takes a viscoelastic instability to grow until an amplitude of $A'(t') = 1$. Similarly, one can define t_{ve} as the time it takes a viscoelastic instability to grow a similar amount. t_{ve} can than be computed using eq. (30).

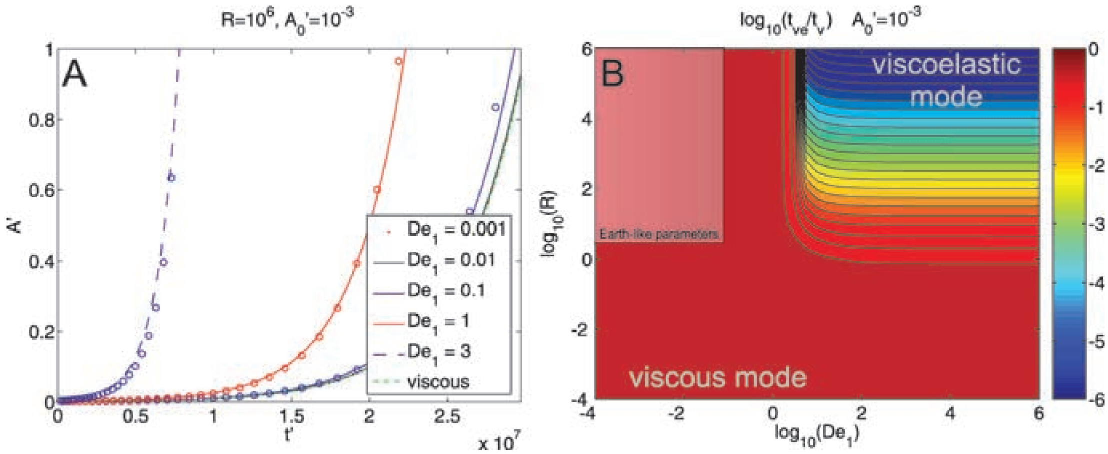

Figure 3. (a) Amplitude–time evolution as a function of Deborah number (De_1) for a viscoelastic layer overlying an infinite viscous half-space, $\lambda/H_1 = 4$, $B_{\rm fac} = 0$. Numerical simulations have been performed for selected cases (open circles, $T = 0.9$). Viscoelastic effects enhance the growth of the RT instability if $De_1 > 0.1$. (b) Contourplot of the time it takes a viscoelastic instability to grow to $A' = 1$ ($t_{\rm ve}$), normalized over the time it would take a viscous instability to reach the same amplitude (t_v). A value of $t_{\rm ve}/t_v = 1$ indicates purely viscous behaviour. Viscoelastic effects enhance the growth of the RT instability, but are present only for sufficiently large values of De_1 and R.

The ratio $t_{\rm ve}/t_v$ is thus an indication of the importance of elasticity for the RT instability. A contourplot of this ratio versus viscosity contrast R and Deborah number De_1 shows that: (a) elasticity enhances the growth of the RT instability and, (b) elasticity has a significant effect on the RT instability only for $De_1 > 1$, $R > 1$ (Fig. 3b). The maximum Deborah number for Earth-like parameters is an order of magnitude smaller than this value ($De_1 = 0.03$, with $\Delta\rho = 330$ kg m^{-3}, $g = 10$ ms^{-2}, $H_1 = 100$ km and $G = 10^{10}$ Pa). Thus, from the analysis presented here, one could conclude that elasticity plays a minor role in lithospheric-scale gravitational instabilities on Earth. In deriving our solution, we however made a number of simplifications. Before drawing any conclusions, we therefore first want to address some of these simplifications.

6.2 Effect of Deborah number, *De*

A combination of numerical and semi-analytical results for a case with a finite-thickness viscous lower layer shows that elasticity increases the growth rate of the RT instability substantially if a critical Deborah number is exceeded (Fig. 4). This is a robust feature and has been observed for a range of boundary conditions and initial set-ups (various T and R); it is also in agreement with previous simulations (Poliakov *et al.* 1993) for the isoviscous case. Intuitively, this effect can be understood by the time dependency of the apparent viscosity in the viscoelastic case as outlined above. Since the apparent viscosity is comparatively small at the beginning of a model run with large *De*, the velocity of the interface is large. With time, the apparent viscosity increases until it approaches the true viscosity and the velocity will decrease. The remarkable agreement between the semi-analytical and numerical solutions (Fig. 4) substantiates this finding. At the onset of the simulation, growth rates are largest (characterized by a sharp increase in amplitude), an effect which is caused by the low apparent viscosity.

The critical Deborah number, $De_{\rm crit}$, is large compared to natural values of *De* ($De \sim 10^{-4} - 1$). This would lead one to expect that the role of elasticity is negligible for Earth-like parameters. However, since $De_{\rm crit}$ is strongly influenced by the boundary and initial conditions, further analysis is useful.

6.3 Growth rate as a function of *De* and *R*

The effects of elasticity on the RT instability can be quantified by computing a growth rate $q_{\rm num}$ from the semi-analytical and numerical simulations as

$$q_{\rm num} = \frac{\log\left((A_{\rm max} + A_0)/A_0\right)}{\Delta t}, \qquad (32)$$

where Δt is the non-dimensional time required for the instability to grow from its initial amplitude A_0 until an amplitude of $A_{\rm max} + A_0$($A_{\rm max} = 0.1H$ is employed here).

A comparison of numerically versus analytically computed growth rates shows excellent agreement (Fig. 5a). At low *De*, elasticity is not important and the growth rate is that of the viscous case with a high-viscosity layer overlying a lower-viscous matrix ($R > 1$). Above a critical *De*, the growth rate increases by several orders of magnitude due to the effects of elasticity until it saturates at a certain level. This saturation growth rate is identical to the viscous growth rate obtained when a low-viscosity layer overlies a higher-viscous matrix. Intuitively this can again be understood by the time dependency of the apparent viscosity of the viscoelastic layer. If viscoelastic effects are important (i.e. *De* is large), the apparent viscosity is small for a significant amount of time. At large *De*, the instability reaches an amplitude of $A = A_{\rm max} + A_0$ before the apparent viscosity of the viscoelastic layer becomes larger than the viscosity of the matrix. Since the growth rate for a viscous set-up with $R < \sim 10^{-4}$ is independent of further changes in R, a saturation effect of $q_{\rm num}$ occurs ($q^{\rm vis}_{\rm max}$).

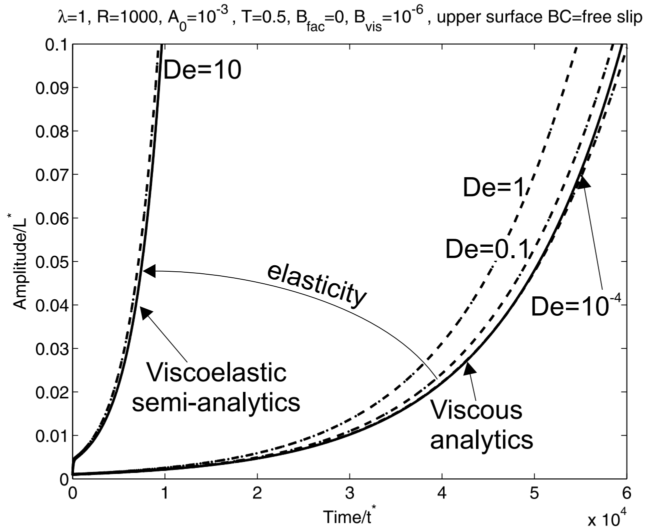

Figure 4. Non-dimensional amplitude versus non-dimensional time as a function of *De* for a fixed wavelength with free-slip upper and lower boundary conditions (other parameters given in the title). Numerical solutions (dashed lines) are in good agreement with semi-analytical solutions (solid lines). Elasticity speeds up the instability above a critical Deborah number of $De_{\mathrm{crit}} \sim 1$.

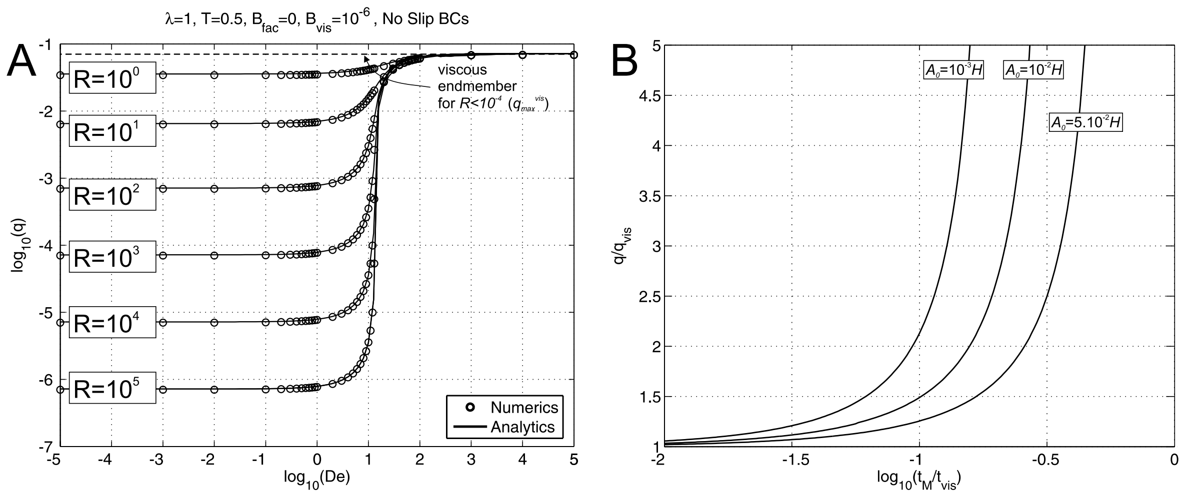

Figure 5. (a) Comparison of numerically and analytically computed growth rate as a function of Deborah number and viscosity contrast for a two-layer system with no-slip lower and upper boundary conditions ($A_0 = 10^{-3}\ H$). (b) Data collapse of (a), showing the speedup of the RT instability due to the effects of elasticity as a function of normalized Maxwell relaxation time of the viscoelastic layer. The characteristic curves are valid for $R > 100$ and arbitrary T, λ and boundary conditions.

The results shown on Fig. 5(a) are computed for a fixed λ, T, A_0 and no-slip boundary conditions; different boundary conditions and initial amplitudes result in different curves. In the following, we describe a more generally applicable technique which results in a set of speedup-curves as a function of a non-dimensional time (or 'effective Deborah number') and initial amplitude. The main advantage of these speedup-curves is that they are no longer dependent on initial and boundary conditions.

The time t_{vis} that a viscous RT instability requires to grow from its initial amplitude A_0 to an amplitude $A_0 + A_{\max}$ is given by

$$t_{\mathrm{vis}} = q_{\mathrm{vis}}^{-1} \log\left(1 + \frac{A_{\max} + A_0}{A_0}\right). \tag{33}$$

This time can be compared with the Maxwell relaxation time of the viscoelastic layer, $t_M = \frac{\mu_1}{G}$, yielding an effective Deborah number,

$$De_{\mathrm{eff}} = \frac{t_M}{t_{\mathrm{vis}}}. \tag{34}$$

Clearly, if $De_{\mathrm{eff}} \gg 1$, viscoelastic effects are expected to be important. An actual computation of the speedup of the RT instability as a function of De_{eff} reveals that, depending on initial amplitude, elasticity influences the RT instability significantly for $De_{\mathrm{eff}} > 0.1$ (Fig. 5b). Although this transition is somewhat dependent on the initial amplitude, it is nearly independent of viscosity contrast, layer thickness, wavelength and boundary conditions (at least for $R > 100$).

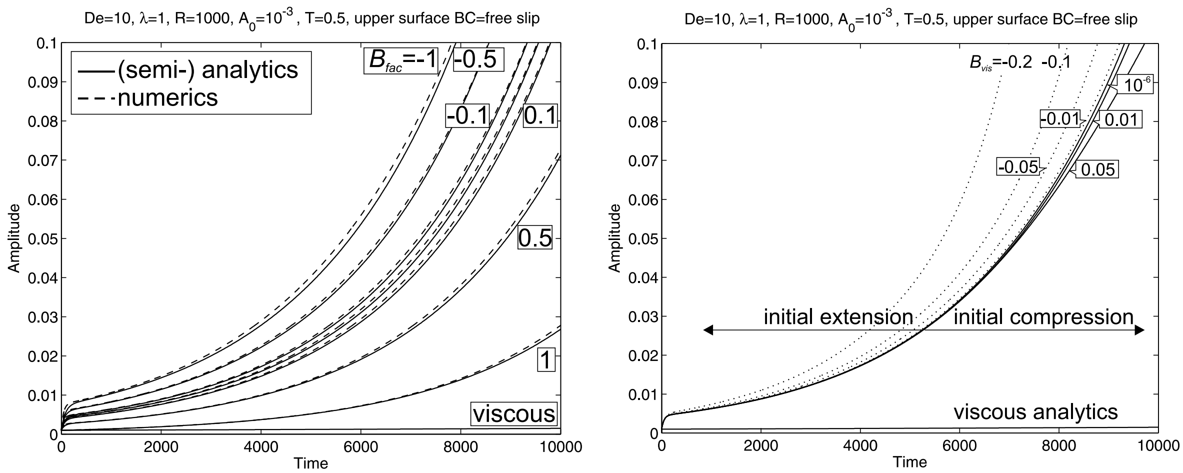

Figure 6. (a) Effect of a gravity-driven pre-stress state on the growth of the instability. Both numerical and analytical solutions are shown. The viscous case ($De \ll 1$) is plotted for comparison. (b) Effect of initial pure-shear compressional state of the system for a two-layer case in which elasticity is important ($De = 10$). All other parameters as in Fig. 4; only numerical solutions are presented. An initial extensional stress state increases the growth rate, whereas an initial compressional stress state decreases the growth rate. Compressional stress states beyond 0.05 resulted in buckling-type instabilities.

6.4 Effect of pre-stress

If elastic effects are significant, the initial stress state of the model influences the growth rate of the instability. We have considered both a gravity- and a compressional-dominated initial stress state. In the first set of models, we consider the effect of a gravity-dominated initial stress state with both numerical and analytical methods (through the parameter B_{fac}). An initial extensional pre-stress ($B_{\mathrm{fac}} < 0$) accelerates the instability whereas an initial compressional stress state ($B_{\mathrm{fac}} > 0$) results in smaller growth rates (Fig. 6). This effect can be understood qualitatively by the time dependency of the apparent viscosity, which is larger for compressional initial stresses.

An interesting effect occurs for $B_{\mathrm{fac}} = 1$, when the initial stress is identical to the viscous stress. We had intuitively expected the growth rate of the viscoelastic RT instability to be identical to that of the viscous case. However, both numerical and analytical results indicate otherwise; they show that the viscoelastic growth rate is significantly larger (Fig. 6) then the viscous growth rate. This is due to the changes in stress caused by the movement of the interface, which results in non-zero elastic strain rates. More quantitatively, we can use the observation that in the viscoelastic case with $B_{\mathrm{fac}} = 1$, amplitudes grows exponential but with a growth rate $q_{\mathrm{ve}} > q_{\mathrm{vis}}$. The temporal evolution of amplitude and stress are then approximately given by

$$A(t) = A_0 e^{q_{ve} t}, \tag{35}$$

$$\tau(t) = \tau_0 e^{q_{ve} t}. \tag{36}$$

Substituting these expressions into the rheological eq. (22) yields the following expression

$$\begin{aligned} \tau_0 q_{ve} &= \frac{2G}{H} A_0 q_{ve} - \frac{G}{\mu_1}\tau_0 \\ q_{ve} &= \frac{\frac{G}{\mu_1}\tau_0}{\frac{2G}{H}A_0 - \tau_0}. \end{aligned} \tag{37}$$

By using $\tau_0 = (2\,\mu_1\, q_{\mathrm{vis}}\, A_0/H)$ for $B_{\mathrm{fac}} = 1$ one can derive a relationship between the viscoelastic growth rate and the viscous growth rate, which is

$$q_{ve} = \frac{1}{1 - \frac{\mu_1}{G} q_{\mathrm{vis}}} q_{\mathrm{vis}} \quad \text{for} \quad 0 < q_{\mathrm{vis}} < \frac{G}{\mu_1}. \tag{38}$$

This expression is similar to the one derived in Poliakov *et al.* (1993). For the case shown on Fig. 6(a) with $B_{\mathrm{fac}} = 1$, $q_{\mathrm{vis}} = 7.74 \times 10^{-5}$, $\mu_1/G = 10^4$. The theoretical speedup ratio of $q_{\mathrm{ve}}/q_{\mathrm{vis}} = 4.42$ compares well with the numerically obtained ratio of 4.32. Eq. (38) has a resonance if $\frac{\mu_1}{G} q_{\mathrm{vis}} \to 1$. In this case, a more complete analysis should be employed to study the behaviour of the model. Examples of such an analysis are the semi-analytical or numerical approaches outlined here. The results indicate that if $\frac{\mu_1}{G} q_{\mathrm{vis}} \geq 1$ the timescale of the deformation becomes controlled by the deformation of the lower, viscous layer. This manifests itself in a stabilization of the growth rate q at large values of De (Fig. 5a). The actual value of this stabilization growth rate ($q^{\mathrm{vis}}_{\mathrm{max}}$) is inversely proportional to the viscosity of the lower layer. A consequence of this is that if the lower layer has zero viscosity, or if it is initially stress free and viscoelastic (resulting in an initially zero apparent viscosity), the above described resonance phenomena may result in an ill-posed problem (with infinite growth rates). We indeed observed un-physical growth rates in cases where the lower layer was viscoelastic and the employed numerical time step was smaller than the smallest relaxation time of the system. For Earth-like parameters, this is not a serious issue since the asthenosphere has a sufficiently small Maxwell relaxation time to be treated as a viscous fluid of small, but finite, viscosity. In a number of papers on the RT instability, however, the mantle has been treated

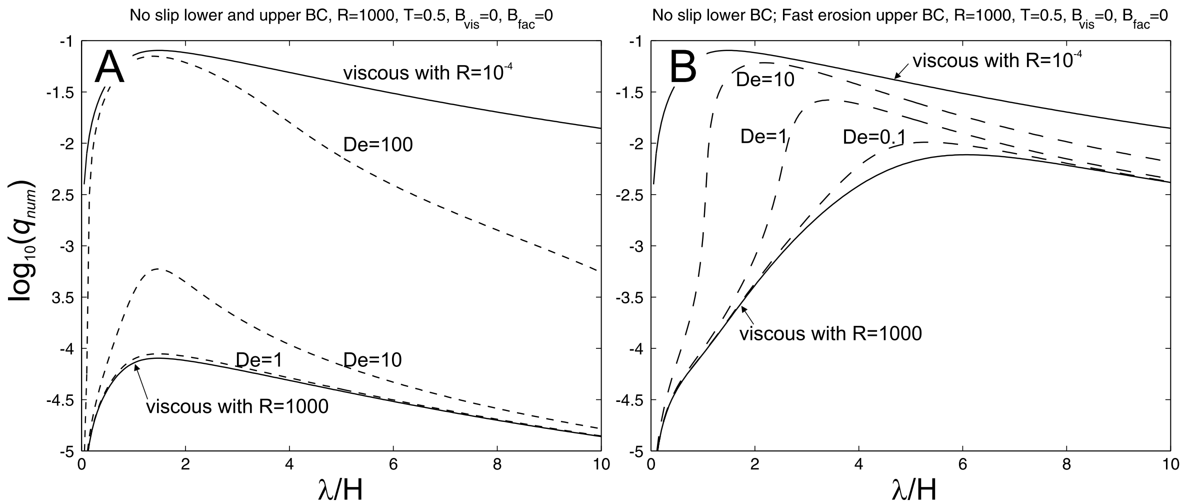

Figure 7. Semi-analytically computed growth rate as a function of wavelength for two different boundary conditions and for different *De*. For comparison, viscous spectra are shown for the case of $R = 1000$ (high-viscosity layer overlying a low-viscosity substratum) and for the case of $R = 10^{-4}$ (limiting case of a weak viscous layer overlying a high-viscosity matrix). With increasing *De*, the viscoelastic growth rate spectra approach the viscous spectra with $R = 10^{-4}$. Note that viscoelastic effects are noticeable for $De = 0.1$ if a fast erosion boundary condition is present, whereas $De > 1$ is required for a no-slip upper boundary condition.

as an inviscid fluid. Whereas this may be a valid approximation if the lithosphere is viscous, caution should be taken when the lithosphere is viscoelastic.

In the second set of models, we consider the effect of an initially far-field compressional or extensional stress state with numerical experiments (through the parameter B_{vis}). In the case of extension ($B_{\text{vis}} < 0$), the growth rate of the RT instability increases compared to initially stress-free models (Fig. 6b). In the case of compression ($B_{\text{vis}} > 0$), on the other hand, the growth rate decreases. However, the effect is less pronounced than in the gravity-dominated case. Our explanation of this is that an initially compressive stress state is not the optimal stress state for a gravity-driven instability. Upon model initialization, a phase of stress re-equilibrium occurs which slows down the instability compared to gravity-driven initial stress states. An additional effect that occurs for far-field initial stress conditions is a buckling, or necking, instability at large values of initial stress.

6.5 Growth rate as a function of wavelength

So far we have shown results for a fixed wavelength of $\lambda/H = 1$. To understand whether and how the dominant wavelength changes as a function of *De* and pre-stress, we have used our semi-analytical solution to compute q_{num} as a function of wavelength and *De* for different boundary conditions (Fig. 7). At low *De*, the growth rate is identical to the viscous case with $R > 1$. The growth rate increases with *De* and approaches that of the viscous case with $R \ll 1$. This saturation effect, which is identical to the effect found in Section 6.3, is caused by the apparent viscosity of the upper layer being very small until the instability reaches an amplitude of $A = 0.1H$.

The dominant wavelength λ_{dom} of the RT instability is typically only weakly dependent on the viscosity contrast (Conrad & Molnar 1997; Kaus 2005). In the case of a fast erosion upper boundary condition, this dependence results in a five-fold reduction of the dominant wavelength, whereas in the case of no-slip boundary conditions the change is hardly noticeable (Fig. 7). The maximum change in dominant wavelength due to the effects of elasticity can thus be estimated by computing λ_{dom} for R and for $R \ll 1$.

6.6 Systematic analysis of De_{crit}

The goal of the present work is to analyse whether, and how, elasticity may influence the dynamics of the RT instability. In the previous sections we demonstrated that elasticity speeds up the RT instability once $De > De_{\text{crit}}$. If De_{crit} is defined as the Deborah number for which $q_{\text{num}} \geq 1.1 q_{\text{vis}}$, we can evaluate the effect of elasticity by computing De_{crit} as a function of viscosity contrast R, initial layer thickness T, initial stress B_{fac}, initial amplitude A_0/H and boundary conditions (Fig. 8). The parameters R and T, as well as boundary conditions, have the largest effect on De_{crit}, whereas both B_{fac} and A_0/H result in second-order modifications only. Maps of De_{crit} as a function of those parameters show that $De_{\text{crit}} \sim 1$ for free-slip and no-slip upper boundary conditions, whereas De_{crit} is somewhat smaller for a free surface and significantly smaller for fast erosion boundary conditions (Fig. 8).

Even though our method of determining De_{crit} overemphasizes the importance of elasticity (q_{num} larger than q_{vis} by 10 per cent), its effect still appears to be small given that for the Earth, $10^{-4} \leq De \leq 1$. If we would have defined De_{crit} as the Deborah number for which $q_{\text{num}} \geq 5 q_{\text{vis}}$, De_{crit} would have been increased by one order of magnitude (see Fig. 5b). The effects of elasticity are thus almost always negligible, the exception being fast erosion upper boundary conditions.

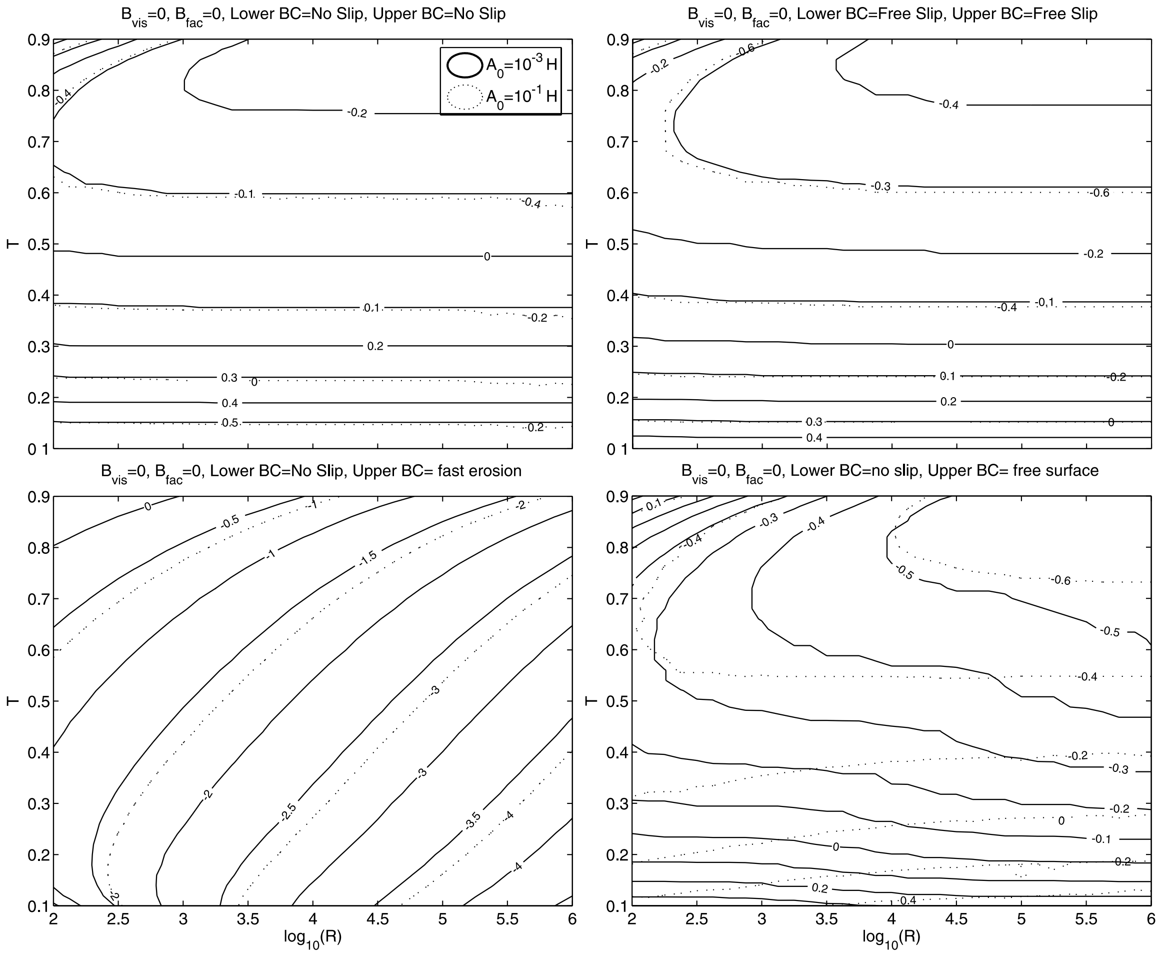

Figure 8. Contours of log $_{10}(De_{\mathrm{crit}})$ versus viscosity contrast R and thickness ratio T for two different initial amplitudes ($D_{\mathrm{surf}} = 0.09$ has been employed in the case of a free-surface upper boundary condition). Computations have been performed for a two-layer system using the semi-analytical solution. The wavelength employed in the computations is the dominant wavelength for the purely viscous case. Variations in the initial stress (from $B_{\mathrm{fac}} = -1$ to $B_{\mathrm{fac}} = 1$) result in smaller variations in De_{crit} than the shown variations in initial amplitude.

7 DETACHMENT OF THE MANTLE LITHOSPHERE IN THE PRESENCE OF A VISCOELASTIC CRUST

Due to its relative cold temperature, the mantle lithosphere is gravitationally unstable with respect to the underlying asthenosphere. Removal of the mantle lithosphere due to a RT instability has been invoked to explain the formation of the Sierra Nevada, California (Lee *et al.* 2000; Jones *et al.* 2004; Molnar & Jones 2004; Zandt *et al.* 2004), Western Tien Shan (Molnar & Houseman 2004), southern Alps of New Zealand (Stern *et al.* 2000; Kohler & Eberhart-Philips 2002), and the western Transverse Ranges, California (Kohler 1999; Billen & Houseman 2004).

We can approximate the detachment problem by a three or few layer viscoelastic fluid model set-up (Figs 9 and 12). Typical material parameters for detachment of the mantle lithosphere (of thickness 50–100 km) are $\Delta\rho = 30$–200 kg m^{-3}, $g = 10$ ms^{-2}, $\mu = 10^{21}$ Pa s, $G = 10^{10}$–10^{11} Pa, $H = 670$ km, where $\Delta\rho$ is the density contrast between lithosphere and mantle (Neil & Houseman 1999; Molnar & Houseman 2004; Molnar & Jones 2004). These yield a Deborah number of $De = 0.002$–0.1, and $T = 0.07$–0.15. Based on our two-layer analysis, these values are too low for elastic effects to have a significant effect on the speed of the downwelling, except if erosion is present (Fig. 8). However, elasticity may have an effect on the stress evolution of the crust as well as on topography above the downwelling; moreover, the presence of a viscoelastic versus a viscous crust effectively changes the upper boundary condition for detachment of the mantle lithosphere which may influence rates of downwelling. In order to quantify such effects, we have performed a series of numerical simulations of a simplified mantle–lithosphere system (Fig. 9). Downwelling of the mantle lithosphere causes deformation and stress build-up in the overlying crust. With our choice of a highly viscous upper crust ($\mu = 10^{25}$ Pa s), $t_M \sim 32$ Myr, thus equal or larger than the timescale of removal of the mantle lithosphere; viscoelastic effects might be important.

The results, for an initially stress-free lithosphere, show a difference in stress amplitude and patterns between viscous, viscoelastic and viscoelastoplastic simulations (Fig. 9). In the viscoelastoplastic simulation, non-associated Mohr–Coulomb plasticity is activated if stresses are above the yield stress (with cohesion $C = 20$ MPa, friction angle $\phi = 30^{\circ}$ and dilation angle $\psi = 0^{\circ}$). The viscous case develops larger stresses, because this model reacts instantaneously to an applied strain rate, whereas stress in the viscoelastic model builds up, or decreases,

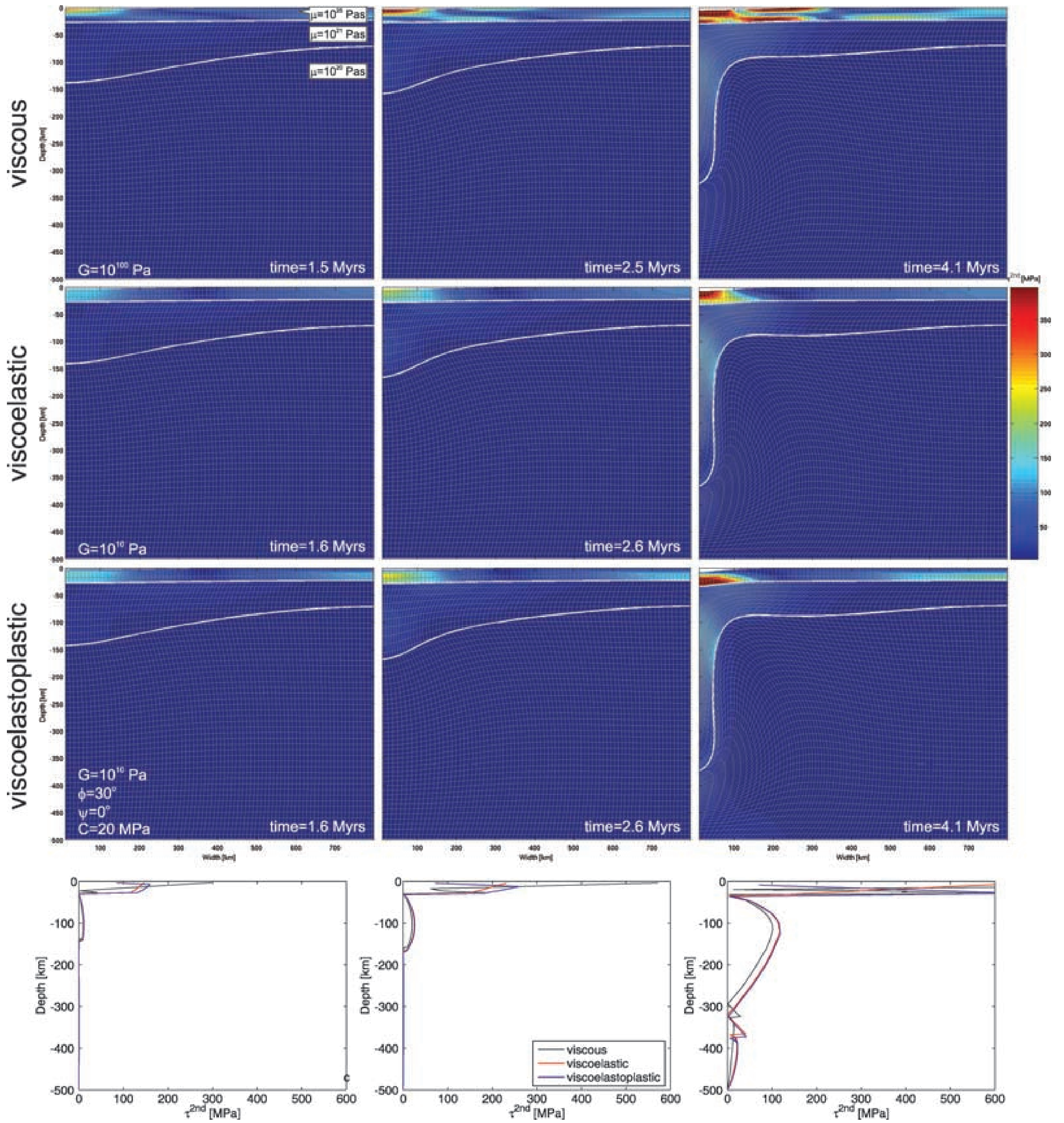

Figure 9. Temporal evolution of the second invariant of the deviatoric stress tensor (differential stress) in models that simulate the detachment of the lower lithosphere as a function of time for a viscous (top), a viscoelastic (middle) and a viscoelastoplastic upper and lower lithosphere. The lowermost panels are vertical cross-sections through the models at 0 km. The top boundary condition is free surface; the bottom boundary condition is no-slip. Thin grey lines indicate passive strain markers and thick white lines rheological boundaries. The lithosphere consists of a crust (with $\rho = 2900$ kg m^{-3} and $\mu = 10^{25}$ Pa s) and a mantle lithosphere (with $\rho = 3300$ kg m^{-3} and $\mu = 10^{21}$ Pa s). The mantle is modelled as a purely viscous fluid (with $\rho = 3100$ kg m^{-3} and $\mu = 10^{20}$ Pa s). The rate at which the lower lithosphere detaches is only slightly larger in the viscoelastic and viscoelastoplastic case; stress evolution and distribution in the crust is, however, significantly different.

more gradually (as a function of the Maxwell relaxation time). The viscoelastic and viscoelastoplastic instabilities are also slightly faster than the viscous case. This is caused by the mechanically weaker viscoelastic crust, which effectively modifies the upper boundary condition of the detachment process. The reduced resistance to flow causes both larger topographic deflections as well as a faster detachment process. Interestingly, the overall dynamics of the viscoelastic and viscoelastoplastic models are fairly similar, suggesting that the main difference with viscous models are due to elasticity. Viscoelastic and viscoelastoplastic models exhibit stress concentrations only above the downwelling, whereas viscous models develop stress perturbations over wider areas. Whereas the stress concentrations above the downwelling are caused

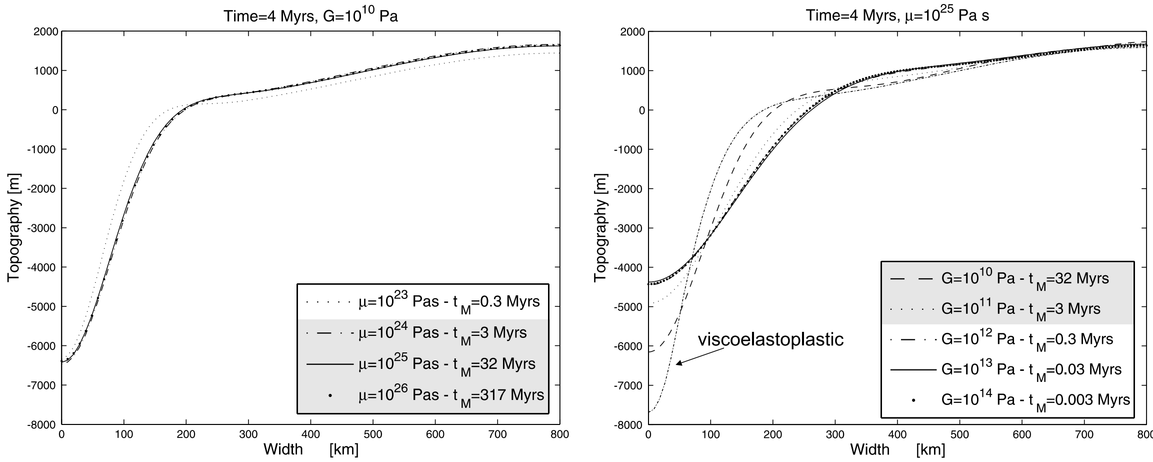

Figure 10. Topography after 4 Myr model evolution for various values of μ (G held fixed; left) and G (μ held fixed; right) of the crust. Viscoelastic effects are noticeable when the Maxwell relaxation time of the crust, t_M, is on the order of 4 Myr or larger (grey areas in legend). Viscoelastic effects increase the topography. The effects of plasticity further increase the topography (results of the viscoelastoplastic model of Fig. 9 with $G = 10^{10}$ Pa are shown).

by vertically dominated flow in this region, stress enhancements at other locations are caused by simple-shear flow of the lithospheric mantle below the mantle–crust interface. In a viscous crust, this shear strain rate is immediately transferred into stress (resulting in a stress field that appears to be elastic), whereas a viscoelastic or viscoelastoplastic crust requires shear to be active for longer times before stress effects are noticeable.

An analysis of the effects of viscoelastic properties of the crust on topography (Fig. 10) reveals that topographic deflections above the downwelling are larger in a viscoelastic crust than in a viscous crust. Plasticity (brittle behaviour) further increases topography, which may be attributed to the effectively weaker crust. Viscoelastic effects are significant only when the timescale of the process is smaller than, or on the same order of, the Maxwell relaxation time of the crust, because the RT instability is sensitive to the apparent viscosity, rather then to the real viscosity. The smaller this apparent viscosity, the larger topographic deflections (Neil & Houseman 1999). Our results suggest that care should be taken when applying viscous RT models to infer the viscosity of the lithosphere using gravity data and topography; ignoring viscoelasticity may result in a underestimation of the true viscosity of the crust and may explain the low values inferred for Venus (Hoogenboom & Houseman 2006), or for the Earth (Billen & Houseman 2004).

Maximum stresses in models with a viscoelastic crust are significantly smaller than in models with an equivalent viscous crust (Fig. 11). Increasing the viscosity of the crust results in an increase of stress until a saturation effect occurs when t_M is significantly larger than the timescale of lithospheric detachment. This result is in agreement with results obtained by Poliakov *et al.* (1993), who studied the interaction between an upwelling diapir and an overlying, viscoelastic crust. Stress reaches a maximum at ∼4 Myr for a high-viscosity crust and at ∼3.7 Myr for a low-viscosity crust and drop afterwards. Differences in timing stem from the fact that a weak crust results in a more deformable upper boundary, enhancing growth of the RT instability.

Our last set of runs highlight the effect of a lower crust on lithosphere–asthenosphere interaction. By varying the viscosity of the lower crust, the coupling between upper crust and mantle lithosphere can be studied. The results (Fig. 12) demonstrate that mantle delamination is significantly faster in the case of a weak lower crust. It also results, as expected, in smaller stresses in the upper crust. Viscous models behave similarly, with the difference that magnitudes of stress are larger. Total detachment occurs after ∼2 Myr for a weak lower crust whereas it may take ∼6 Myr for a viscosity of the lower crust which is similar, or larger, than the viscosity of the mantle lithosphere (Fig. 13).

8 DISCUSSION

Elasticity may enhance the growth of the RT instability. Whether this effect is important for lithospheric deformation or not is critically dependent on the speed of the viscous counterpart of the instability. If the viscous instability grows to finite amplitudes at a timescale smaller than the Maxwell relaxation time of the layer, viscoelasticity will most likely enhance the growth of the instability.

We have made a number of simplifying assumptions. For example, the rheology of rocks is Newtonian, which is only valid for the low-stress diffusion creep regime. Most likely, the rheology of rocks under lithospheric-scale conditions is rather governed by power-law or non-Newtonian creep. The effect of such a rheology on the RT instability was studied in detail by Conrad & Molnar (1997). They found that the growth rate of a non-Newtonian layer overlying an infinite half-space is given in dimensional units by

$$q_{\mathrm{NonNew}} = \frac{(\rho_1 - \rho_2) g H_1 C}{\mu_1}, \tag{39}$$

where C is the maximum growth rate in non-dimensional units which varies from 0.16 in the Newtonian case to 0.59 in the case of a perfectly plastic layer. Superexponential growth (or 'blowup') occurs once the instability has reached an amplitude approximately equal to the initial

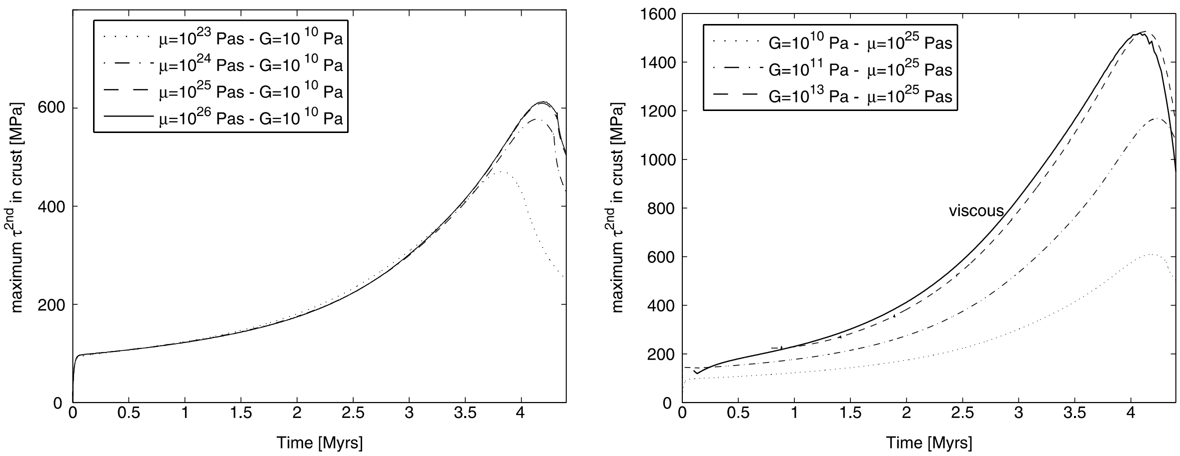

Figure 11. Temporal evolution of maximum differential stress in the crust for various values of μ (left) and G (right) in the crust. Viscoelastic effects result in smaller values of stress compared to purely viscous models. In the Earth's lithosphere $G = 10^{10}$–10^{11} Pa.

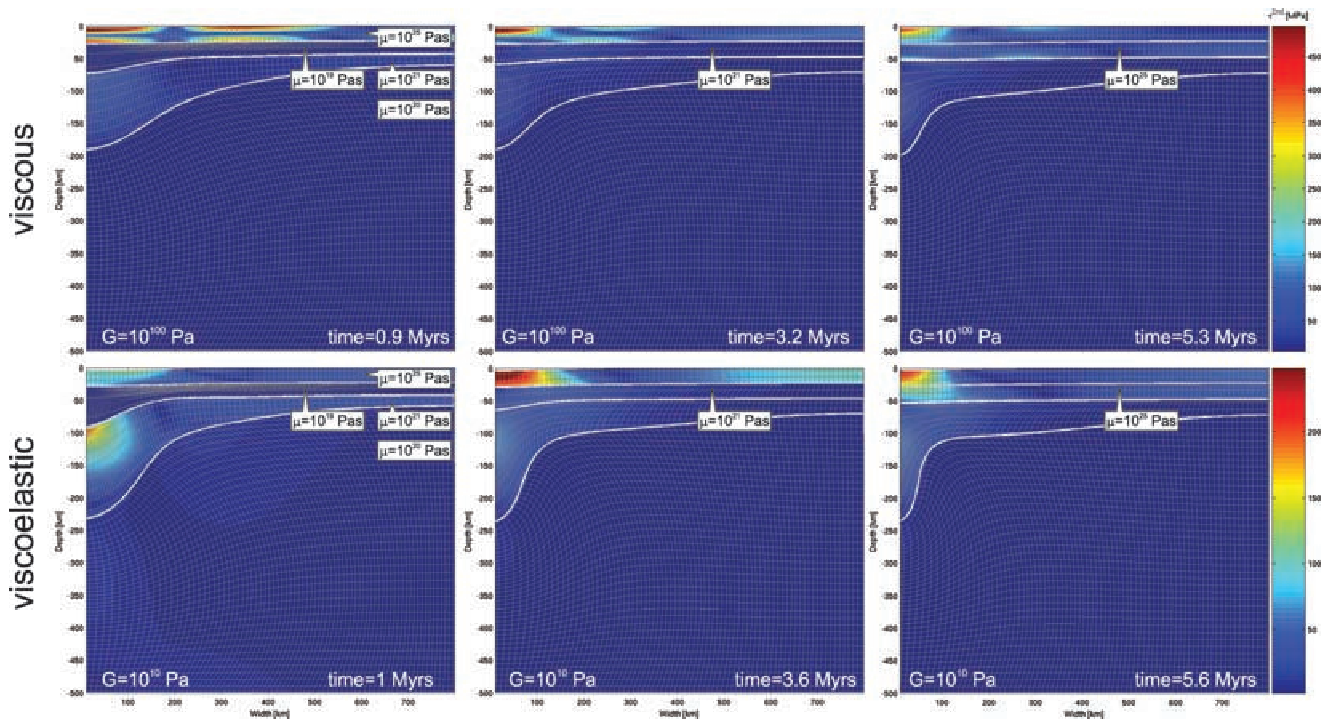

Figure 12. Deviatoric stress for models that include a lower crust of 25 km thickness with the same density as the upper crust but different viscosity. All other properties as in Fig. 9. Top panels are for a purely viscous rheology whereas bottom panels take lithospheric elasticity into account. A weak lower crust (left panels) results in smaller stresses and faster detachment rates compared to models in which the strength of the lower crust is equal to that of the mantle or to that of the crust (right panels). Viscous models develop larger stresses. The scales of the colour bars are different.

layer thickness H_1. The time t_{vis} to reach this thickness is thus given by

$$t_{\text{vis}} = \frac{\log\left(\frac{H_1}{A_0}\right)}{q_{\text{vis}}}. \tag{40}$$

An indication of the importance of elasticity is given by the ratio of the viscous growth time with the Maxwell relaxation time (see Section 6.3; Fig. 5b).

$$\frac{t_M}{t_{\text{vis}}} = \frac{(\rho_1 - \rho_2) g H_1 C}{\log\left(\frac{H_1}{A_0}\right) G}. \tag{41}$$

For $(\rho_1 - \rho_2) = 200$ kg m^{-3}, $g = 10$ ms^{-2}, $H_1 = 160$ km, $G = 10^{10}$ Pa and $H_1/A_0 = 0.01$–0.1, we obtain $t_M/t_{\text{vis}} = 1.1 \times 10^{-3}$–$8 \times 10^{-3}$. According to the analysis presented in this work, t_M/t_{vis} should be larger than $\sim 10^{-2}$ for elasticity to have a noticeable, and larger than $\sim 10^{-1} - 1$ for a significant, effect (Fig. 5b). It seems unlikely that elastic effects will significantly alter the results of Conrad & Molnar (1997).

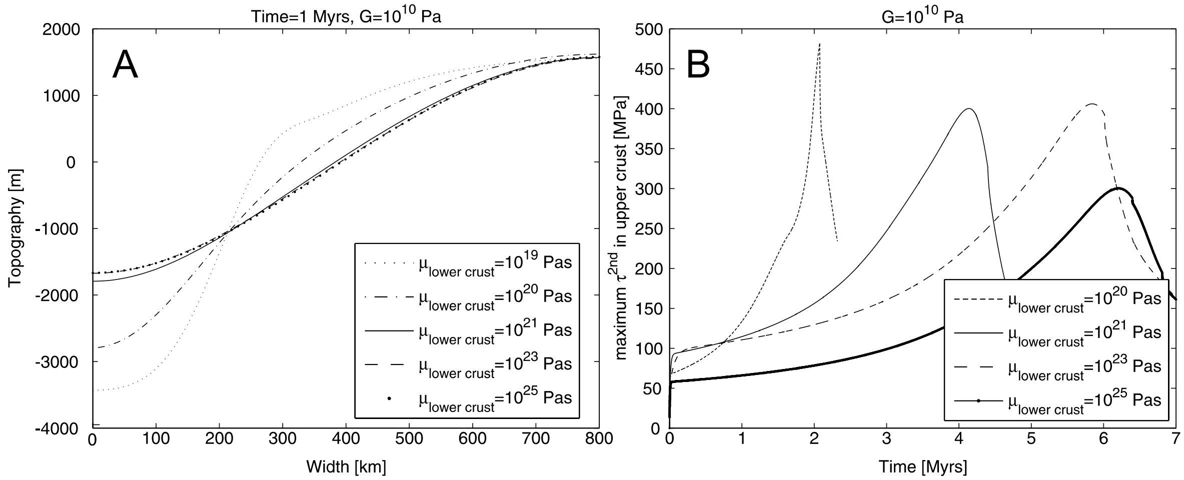

Figure 13. (a) Surface topography after 1 Myr. The weaker the lower crust, the faster the detachment and the larger the topographic deflections above the downwelling mantle lithosphere. (b) Temporal evolution of maximum differential stress in models where a lower crust is present (*cf.* Fig. 12). A weak lower crust results in a faster stress increase than cases with a strong crust.

Another effect that has been ignored here is the effect of horizontal shortening. Compression in the presence of a free surface may result in lithospheric-scale buckling (Burg & Podladchikov 1999; Toussaint *et al.* 2004; Schmalholz *et al.* 2005), which may result in larger initial perturbations. The effects of folding or buckling have previously been eliminated in most studies on lithospheric detachment by imposing a free slip, or constant velocity, upper boundary condition. A study by Burg *et al.* (2004; see also Kaus 2005) allowed for folding (in the presence of fast erosion) and showed that folding will dominate over the RT instability if initial amplitudes are small and

$$\left(\frac{\mu_1}{\mu_2}\right)^{\frac{2}{3}} \dot{\varepsilon}_{BG} > 0.39\frac{(\rho_1-\rho_2)g(H-H_1)}{2\mu_2}, \tag{42}$$

where $\dot{\varepsilon}_{BG}$ is the applied background strain rate. Employing $(\rho_1 - \rho_2) = 30 - 200$ kg m^{-3}, $g = 10$ ms^{-2}, $(H - H_1) = 500$ km, $\mu_2 = 10^{20}$ Pa s suggests that folding will dominate over the RT instability if $\mu_1 > 5 \times 10^{23}$–3×10^{26} Pa s for values of $\dot{\varepsilon}_{BG} = 10^{-15}$–$10^{-16}$s^{-1}. This estimate, however, ignores the effects of elasticity, which have been demonstrated to greatly enhance the growth of the buckling instability (Schmalholz & Podladchikov 1999; Schmalholz *et al.* 2002).

In order to keep the number of free parameters to a minimum, we have ignored the effects of plastic yielding throughout most of this work. Clearly, this is an oversimplification since in the lithosphere deforms in a plastic fashion if differential stresses exceed the brittle yield strength of rocks. Stresses that develop in the RT instability are proportional to the buoyancy force, given by $\Delta\rho g H$. Reasonable parameters result in (maximum) 100 MPa in most regions, confirmed by numerical experiments (Figs 9 and 12). These values are lower than the typical yield strength of mantle rocks inferred from laboratory experiments (∼500 MPa). Magnitudes of stress obtained in the crust exceed the values obtained in the mantle lithosphere (caused by the stress-focussing effect; Podladchikov *et al.* 1993; Vasilyev *et al.* 2001). Here, brittle failure occurs above the downwelling mantle lithosphere. Indeed, simulations in which plasticity is taken into account show brittle behaviour at this location (Fig. 9). Compared with the effects of elasticity, the overall effect of plasticity is small. Plasticity does, however, influence topography (see Fig. 9 and Burov & Guillou-Frottier 2005).

Moresi *et al.* (2002) described a numerical methodology and applied it to mantle convection in the presence of visco-elasto-plastic plates. They presented three convection simulations which suggested that the elasticity may have the possible side-effect of causing slabs to roll-back instead of to move forwards. Since they also included strain weakening it is not entirely clear whether this effect can be completely attributed to the effects of elasticity.

Recently, Mühlhaus & Regenauer-Lieb (2005) numerically studied the effects of elasticity (in combination with plasticity) on mantle convection. They showed that the general patterns of convection are not significantly altered by the presence of elasticity; it, however, decreases the amount of dissipation in the lithosphere. These authors also showed an increase in convection speed with decreasing elastic shear module. In agreement with our results here, they found that the parameters required for this effect to occur are unrealistic for the Earth.

9 CONCLUSIONS

In order to estimate the importance of elasticity on gravity-driven instabilities we studied the effect of elasticity on the RT instability. To summarize our findings:

(i) If elasticity is important, it enhances the growth of the RT instability which appears sensitive to the viscous part of deformation only. If the timescale of the process is smaller than the Maxwell relaxation time, the elastic part of the deformation is non-negligible. In this case, elasticity transforms a seemingly strong layer (i.e. with large viscosity) into a transiently weak layer, causing deformation to occur significantly faster.

(ii) We have derived both an analytical and a semi-analytical model for the viscoelastic RT instability which reproduces numerical results up to finite amplitudes with remarkable accuracy.

(iii) The solutions are employed to study the importance of elasticity for Earth-like parameters and boundary conditions; results indicate that the effect of elasticity is negligible in most cases. Only the presence of a free surface (preferably one that is being rapidly eroded) may result in a slight speedup of the instability.

(iv) Numerical simulations of multilayer detachment processes of the mantle lithosphere with a free surface indicate that stresses are lower in a viscoelastic crust than in a viscous crust. Topographies and rates of downwellings are larger when a viscoelastic or a viscoelastoplastic crust is present.

The question of whether elasticity is important for geodynamics or not cannot be answered with a simple yes or no. In this study, we demonstrated that elastic effects, on the one hand, have a negligible effect on the dynamics of the RT instability. On the other hand, we also showed that stress builds up differently in viscoelastic models compared to viscous models. Other workers have pointed out that elasticity is important for compressional-driven instabilities (e.g. Schmalholz & Podladchikov 1999) and for shear localization (Ogawa 1987; Kaus & Podladchikov 2006). Both processes depend on the state of stress of the lithosphere, which is currently not well understood. Future numerical and analytical work is thus required to better understand the effects of elasticity (and plasticity) on actively deforming parts of the lithosphere. By doing this, we will potentially be able to relate the effective elastic thickness to the thermal, mechanical and dynamical state of the lithosphere. We could also answer questions such as whether the apparent absence of earthquakes in the mantle lithosphere is indeed caused by a weak rheology of mantle rocks (Jackson 2002) or whether the 'Christmas-tree' strength envelops simply overestimates differential stresses of the mantle lithosphere (Schmalholz *et al.* 2005; Kaus & Schmalholz 2006; Regenauer-Lieb *et al.* 2006).

ACKNOWLEDGMENTS

Computations have been performed at the high-performance supercomputer centre of the University of Southern California. We thank Yuri Podladchikov, Evgenii Burov, Peter Molnar for discussions, the editor Harro Schmeling, an anonymous reviewer and Gabriele Morra for reviews, and Laetitia Le Pourhiet for numerous discussions and for her willingness to compare the results of different numerical codes for set-ups and rheologies similar to the ones presented in this work.

REFERENCES

Bassi, G. & Bonnin, J., 1988. Rheological modeling and deformation instability of lithosphere under extension, *Geophys. J.,* **93,** 485–504.

Batt, G.E. & Braun, J., 1997. On the thermomechanical evolution of compressional orogens, *Geophys. J. Int.,* **128,** 364–382.

Bercovici, D., Dick, H. & Wagner, T., 1992. Nonlinear viscoelasticity and the formation of transverse ridges, *J. geophys. Res.,* **97,** 14 195–14 206.

Billen, M.I. & Houseman, G., 2004. Lithospheric instability in obliquely convergent margins: San Gabriel Mountains, Southern California, *J. geophys. Res.,* **109,** doi:10.1029/2003JB002605.

Biot, M., 1965. *Mechanics of Incremental Deformations,* John Wiley and Sons, New York.

Biot, M. & Odé, H., 1965. Theory of gravity instability with variable overburden and compaction, *Geophysics,* **30,** 153–166.

Braun, J. & Sambridge, M., 1994. Dynamic Lagrangian Remeshing (DLR): a new algorithm for solving large strain deformation problems and its application to fault-propagation folding, *Earth planet. Sci. Lett.,* **124,** 211–220.

Buiter, S.J.H., Babeyko, A., Ellis, S., Gerya, T., Kaus, B., Kellner, A., Schreurs, G. & Yamada, Y., 2006. The numerical sandbox: comparison of model results for a shortening and an extension experiment., in *Analogue and Numerical Modelling of Crustal-Scale Processes,* **Vol. 253,** pp. 29–64, eds Buiter, S.J.H. & Schreurs, G., of Geological Society of London Special Publications, Geological Society of London.

Burg, J.P. & Podladchikov, Y., 1999. Lithospheric scale folding: numerical modeling and application to the himalayan syntaxes, *Int. J. Earth Sc.,* **88**(2), 190–200.

Burg, J.P., Kaus, B. & Podladchikov, Y., 2004. Dome structures in collision orogens. Mechanical investigation of the gravity/compression interplay, in *Gneiss Domes in Orogeny,* **Vol. 380,** pp. 47–66, eds Whitney, D., Teyssier, C. & Siddoway, C., Geological Society of America, Boulder.

Burov, E. & Guillou-Frottier, L., 2005. The plume head-continental lithosphere interaction using a tectonically realistic formulation for the lithosphere, *Geophys. J. Int.,* pp. doi:10.1111/j.1365–246X.2005.02588.x.

Conrad, C. & Molnar, P., 1997. The growth of Rayleigh-Taylor-type instabilities in the lithosphere for various rheological and density structures, *Geophys. J. Int.,* **129,** 95–112.

Cuvelier, C., Segal, A. & van Steenhoven, A., 1986. *Finite Element Methods and Navier-Stokes Equations, Mathematics and its Applications,* Reidel Publishing company, Dordrecht.

Dziewonski, A. & Anderson, D.L., 1981. Preliminary reference Earth model, *Phys. Earth Planet. Inter.,* **25,** 297–356.

Fletcher, R.C., 1972. Application of a mathematical-model to emplacement of mantled gneiss domes, *American Journal of Science,* **272**(3), 197–216.

Fletcher, R.C. & Hallet, B., 1983. Unstable extension of the lithosphere: a mechanical model for basin-and-range structure, *J. geophys. Res.,* **88**(B9), 7457–7466.

Frederiksen, S. & Braun, J., 2001. Numerical modeling of strain localisation during extension of the continental lithosphere, *Earth planet. Sci. Lett.,* **188,** 241–251.

Funiciello, F., Morra, G., Regenauer-Lieb, K. & Giardini, D., 2003. Dynamics of retreating slabs (part 1): insights from 2-D numerical experiments, *J. geophys. Res.,* **108**(B4), 2206, doi:10.1029/2001JB000898.

Gerbault, M., 2000. At what stress level is the Central Indian Ocean lithosphere buckling?, *Earth Planet. Sci. Lett.,* **178**(1–2), 165–181.

Gurnis, M., Eloy, C. & Zhong, S., 1996. Free-surface formulation of mantle convection- ii. Implications for subduction zone observables, *Geophys. J. Int.,* **127,** 719–727.

Hall, C.E. & Gurnis, M., 2005. Strength of fracture zones from their barythmetic and gravitational evolution, *J. geophys. Res.,* **110**(B01402), doi:10.1029/2004JB003312.

Hall, C.E., Gurnis, M., Sdrolias, M., Lavier, L. & Dietmar Mueller, R., 2003. Catastrophic initiation of subduction following forced convergence across fracture zones, *Earth Planet. Sci. Lett.,* **212,** 15–30.

Harder, H., 1991. Numerical simulation of thermal convection with Maxwellian viscoelasticity, *Journal of Non-Newtonian Fluid Mechanics,* **39,** 67–88.

Hoogenboom, T. & Houseman, G., 2006. Rayleigh-Taylor instability as a mechanism for corona formation on Venus, *Icarus,* **180,** 292–307.

Ivins, E.R., Unti, T. & Phillips, R., 1982. Large Prandtl number finite-amplitude thermal-convection with Maxwell viscoelasticity, *Geoph. Astroph. Fluid Dyn.,* **22**(1-2), 103–132.

Jackson, J., 2002. Strength of the continental lithosphere: time to abandon the jelly sandwich?, *GSA Today,* **September,** 4–10.

Jones, C.H., Farmer, G.L. & Unruh, J.R., 2004. Tectonics of Pliocene removal of lithosphere of the Sierra Nevada, California, *Geol. Soc. Am. Bull.,* **116,** 1408–1422.

Kaus, B., 2005. *Modelling approaches to geodynamic processes,* Phd-Thesis, Swiss Federal Institute of Technology, (http://geodynamics.usc.edu/∼bkaus/PhD \ _Kaus \ _Doublesided.pdf.

Kaus, B. & Schmalholz, S.M., 2006. 3D Finite amplitude folding: implications for stress evolution during crustal and lithospheric deformation., *Geophys. Res. Lett.,* **33**(L14309), doi:10.1029/2006GL026341.

Kaus, B., Podladchikov, Y. & Schmid, D.W., 2004. Eulerian spectral/finite difference method for large deformation modelling of visco-elasto-plastic geomaterials, *Bolletino Geofisico,* **45,** 346–349.

Kaus, B.J.P. & Podladchikov, Y., 2006. Initiation of localized shear zones in viscoelastoplastic rocks., *J. geophys. Res.,* **111**(B04412), doi:10.1029/2005JB003652.

Kohler, M., 1999. Lithospheric deformation beneath the San Gabriel Mountains in the southern California Transverse Ranges, *J. geophys. Res.,* **104,** 15 025–15 041.

Kohler, M. & Eberhart-Philips, D., 2002. Three-dimensional lithospheric structure below the New Zealand Southern Alps, *J. geophys. Res.,* **107,** 2225, doi:10.1029/2001JB000182.

Lee, C.-T., Yin, Q.-Z., Rudnick, R., Chesley, J. & Jacobsen, S., 2000. Osmium isotope evidence for Mesozoic removal of the lithospheric mantle beneath the Sierra Nevada, California, *Science,* **289,** 1912–1916.

Mancktelow, N.S., 2001. Single-layer folds developed from initial random perturbations: the effects of probability distribution, fractal dimension, phase, and amplitude, in *Tectonic Modeling: A Volume in Honor of Hans Ramberg,* **Vol. 193,** pp. 69–87, eds Koyi, H. & Mancktelow, N.S., Geological Society of America, Boulder, CO.

Melosh, H.J., 1978. Dynamic support of the outer rise, *Geophys. Res. Lett.,* **5,** 321–324.

Molnar, P. & Houseman, G., 2004. The effects of buoyant crust on the gravitational instability of thickened mantle lithosphere at zones of intracontinental convergence, *Geophys. J. Int.,* **158,** 1134–1150, doi:10.1111/j.1365–46X.2004.02312.x.

Molnar, P. & Jones, C., 2004. A test of laboratory based rheological parameters of olivine from an analysis of late Cenozoic convective removal of mantle lithosphere beneath the Sierra Nevada, California, USA, *Geophys. J. Int.,* **2004**(156), 555–564, doi:10.1111/j.1365–246X.2004.02138.x.

Moresi, L., Dufour, F. & Muehlaus, H.B., 2002. Mantle convection modeling with viscoelastic/brittle lithosphere: numerical modeling and plate tectonic modeling, *Pure appl. Geophys.,* **159,** 2335–2356.

Moresi, L., Dufour, F. & Muhlhaus, H.-B., 2003. A Lagrangian integration point finite element method for large deformation modeling of viscoelastic geomaterials, *Journal of Computational Physics,* **184,** 476–497.

Mühlhaus, H.B. & Regenauer-Lieb, K., 2005. A self-consistent plate mantle model that includes elasticity: computational aspects and application to basic modes of comvection, *Geophys. J. Int.,* doi:10.1111/j.1365–246X.2005.02742.x.

Naimark, B.M. & Ismail-Zadeh, A., 1994. Gravitational instability of Maxwell upper mantle, *Comput. Seis. Geodyn.,* **1,** 36–42.

Neil, E. & Houseman, G., 1999. Rayleigh-Taylor instability of the upper mantle and its role in intraplate orogeny, *Geophys. J. Int.,* **138,** 89–107.

Odé, H., 1966. Gravitational instability of a multilayered system of high viscosity, *Verhandelingen der Koninklijke Nederlandse Akademie van Wetenschappen, Afd. Natuurkunde.,* **1**(24), 96.

Ogawa, M., 1987. Shear instability in a viscoelastic material as the cause of deep focus earthquakes, *J. geophys. Res.,* **92**(B1), 13 801–13 810.

Peltier, W.R., 1985. Mantle convection and viscoelasticity, *Ann. Rev. Fluid Mech.,* **17,** 561–608.

Podladchikov, Y., Lenardic, A., Yuen, D. & Quareni, F., 1993. Dynamical consequences of stress focussing for different rheologies: Earth and Venus perspectives, *EOS, Trans. Am. geophys. Un.,* **74**(43), 566.

Poliakov, A. & Podladchikov, Y., 1992. Diapirism and topography, *Geophys. J. Int.,* **109,** 553–564.

Poliakov, A., Cundall, P., Podladchkov, Y. & Lyakhovsky, V., 1993. An explicit inertial method for the simulation of viscoelastic flow: an evaluation of elastic effects on diapiric flow in two- and three- layers models, in *Flow and Creep in the Solar System: observations, modeling and Theory,* pp. 175–195, eds Stone, D. & Runcorn, S., Proceeding of NATO Advanced Study. Institute.

Ranalli, G., 1995. *Rheology of the Earth,* 2nd edn, Chapman and Hall, London.

Regenauer-Lieb, K., Yuen, D. & Branlund, J., 2001. The initation of subduction: criticality by addition of water?, *Science,* **294,** 578–580.

Regenauer-Lieb, K., Weinberg, R.F. & Rosenbaum, G., 2006. The effect of energy feedbacks on continental strength, *Nature,* **442,** doi:10.1038/nature04868.

Ricard, Y. & Froidevaux, C., 1986. Stretching instabilities and lithospheric boudinage, *J. geophys. Res.,* **91**(B8), 8314–8324.

Schmalholz, S.M. & Podladchikov, Y., 1999. Buckling versus folding: importance of viscoelasticity, *Geophys. Res. Lett.,* **26**(17), 2641–2644.

Schmalholz, S.M. & Podladchikov, Y.Y., 2001. Viscoelastic folding: Maxwell versus kelvin rheology, *Geophys. Res. Lett.,* **28**(9), 1835–1838.

Schmalholz, S.M., Podladchikov, Y.Y. & Schmid, D.W., 2001. A spectral/finite difference method for simulating large deformations of heterogeneous, viscoelastic materials, *Geophys. J. Int.,* **145**(1), 199–208.

Schmalholz, S.M., Podladchikov, Y. & Burg, J.P., 2002. Control of folding by gravity and matrix thickness: implications for large-scale folding, *J. geophys. Res.,* **107,** doi:10.1029/2001JB000355.

Schmalholz, S.M., Podladchikov, Y. & Jamtveit, B., 2005. Structural softening of the lithosphere, *TerraNova,* **17,** 66–72, doi:10.1111/j.1365–3121.2004.00585.x.

Schubert, G., Olson, P. & Turcotte, D.L., 2001. *Mantle convection in the Earth and planets,* Cambridge University Press, Cambridge.

Stern, T., Molnar, P., Okaya, D. & Eberhart-Philips, D., 2000. Teleseismic P wave delays and modes of shortening the mantle lithosphere beneath South Island, New Zealand, *J. geophys. Res.,* **105,** 21 615-21 632.

Toth, G. & Gurnis, M., 1998. Dynamics of subduction initiation at preexisting fault zones, *J. geophys. Res.,* **103,** 18 053–18 067.

Toussaint, G., Burov, E. & Jolivet, L., 2004. Continental plate collision: unstable vs. stable slab dynamics, *Geology,* **32**(1), 33–36.

Vasilyev, O.V., Podladchikov, Y.Y. & Yuen, D.A., 2001. Modeling of plume-lithosphere interaction using adaptive multilevel wavelet collocation algorithm., *Geophys. J. Int.,* **147**(3), 579–589.

Zandt, G., Gilbert, H., Owens, T., Ducea, M., Saleeby, J. & Jones, C.H., 2004. Active foundering of a continental arc root beneath the southern Sierra Nevada, California, *Nature,* **431,** 41–46.

Zuber, M.T., Parmentier, E.M. & Fletcher, R.C., 1986. Extension of the continental lithosphere: a model for two scales of Basin and Range deformation, *J. geophys. Res.,* **91**(B5), 4826–4838.

APPENDIX A: LINEAR STABILITY ANALYSIS

The semi-analytical solution derived here consists of a set of ordinary differential equations that are coupled to a classical growth rate analysis for the purely viscous RT instability. Viscoelasticity enters the problem by modifying the viscosity as a function of stress level (i.e. the apparent viscosity rather than the true viscosity is employed). Since in our model only the upper layer is viscoelastic, the apparent viscosity is only employed for this layer; the lower layer has a Newtonian viscosity at all times. Here we outline the solution method for the viscous RT instability. The derivation closely follows previous workers (Biot & Odé 1965; Fletcher 1972; Bassi & Bonnin 1988; Conrad & Molnar 1997; Fletcher & Hallet 1983; Ricard & Froidevaux 1986; Zuber *et al.* 1986; Burg *et al.* 2004). It differs, however, in the way we treat the time stepping which is done with an implicit rather than explicit method, resulting in a large stability improvement when a free surface is present.

The incompressibility and force balance equations in 2-D are:

$$\frac{\partial V_x}{\partial x} + \frac{\partial V_z}{\partial z} = 0, \tag{A1}$$

$$\frac{\partial \sigma_{xx}}{\partial x} + \frac{\partial \sigma_{xz}}{\partial z} = 0, \tag{A2}$$

$$\frac{\partial \sigma_{xz}}{\partial x} + \frac{\partial \sigma_{zz}}{\partial z} = \rho g, \tag{A3}$$

where V_x, V_z denotes velocity in x, z-direction, ρ density, g gravity, P pressure and σ_{xx}, σ_{zz}, σ_{xz} stress. Stress is related to deviatoric stress as:

$$\sigma_{xx} = \tau_{xx} - P, \tag{A4}$$

$$\sigma_{zz} = \tau_{zz} - P, \tag{A5}$$

$$\sigma_{xz} = \tau_{xz}. \tag{A6}$$

Strain rates are defined as:

$$\dot{\varepsilon}_{xx} = \frac{\partial V_x}{\partial x}, \tag{A7}$$

$$\dot{\varepsilon}_{zz} = \frac{\partial V_z}{\partial z}, \tag{A8}$$

$$\dot{\varepsilon}_{xz} = \frac{1}{2}\left(\frac{\partial V_x}{\partial z} + \frac{\partial V_z}{\partial x}\right). \tag{A9}$$

The rheology for deviatoric stresses is viscous,

$$\tau_{ij} = 2\mu_{\text{app}}\dot{\varepsilon}_{ij}, \tag{A10}$$

where μ_{app} is the apparent viscosity (see eq. 5) of the viscoelastic layer or the true viscosity of the viscous layer. Furthermore, it is assumed that pressure and velocities vary harmonically in the horizontal direction:

$$V_z(x, z) = v_z(z)\cos(kx), \tag{A11}$$

$$V_x(x, z) = -\frac{v_x(z)}{k}\sin(kx), \tag{A12}$$

$$P(x, z) = p(z)\cos(kx), \tag{A13}$$

where $k = 2\pi/\lambda$ is the wavenumber, and λ the wavelength. Substituting eqs (A11) and (A12) into eq. (A1) yields an explicit expression of v_x as a function of v_z. Pressure can be eliminated from eqs (A2) and (A3), by taking the derivative of eq. (A2) versus z and subtracting the derivative of eq. (A3) versus x. The resulting equation is a fourth-order differential equation for $v_z(z)$.

$$\frac{\partial^4 v_z(z)}{\partial z^4} - 2k^2\frac{\partial^2 v_z(z)}{\partial z^2} + k^2 v_z(z) = 0. \tag{A14}$$

The solution of this equation has the form:

$$\begin{aligned} v_z(z) = {} & A\exp(kz) + B\exp(kz)z \\ & + C\exp(-kz) + D\exp(-kz)z, \end{aligned} \tag{A15}$$

where $A - D$ are to-be-determined constants. From eq. (A15), which is valid inside each layer, we can determine analytical expressions for v_x, τ_{xx}, τ_{xz}, τ_{zz}, σ_{xx}, σ_{xz}, σ_{zz} and P.

We study two layers, with fixed or free surface. We thus have eight unknown coefficients for which we need eight additional equations. Four of those are given at the interface between the two layers (e.g. at $z = H_{\text{int}}$). A first-order Taylor expansion around $z = H_{\text{int}}$ gives an expression for the continuity of velocity

$$\begin{aligned} & v_z^1(H_{\text{int}}) - v_z^2(H_{\text{int}}) = 0 \\ & v_x^1(H_{\text{int}}) - v_x^2(H_{\text{int}}) = 0. \end{aligned} \tag{A16}$$

Continuity of shear and normal stresses are given by

$$\begin{aligned} & \sigma_{xz}^1(H_{\text{int}}) - \sigma_{xz}^2(H_{\text{int}}) = 0 \\ & \sigma_{zz}^1(H_{\text{int}}) - \sigma_{zz}^2(H_{\text{int}}) = (\rho_1 - \rho_2)gA, \end{aligned} \tag{A17}$$

where A is the amplitude of the sinusoidal perturbation of the interface. The four other equations are obtained from the boundary conditions. No-slip conditions at the bottom of the domain are given by

$$\begin{aligned} v_x^2(0) &= 0 \\ v_z^2(0) &= 0. \end{aligned} \tag{A18}$$

Alternatively we can have free-slip lower boundary conditions

$$\begin{aligned} v_z^2(0) &= 0 \\ \sigma_{xz}^2(0) &= 0. \end{aligned} \tag{A19}$$

A no-slip condition at the top of the domain is given by

$$\begin{aligned} v_x^1(H) &= 0 \\ v_z^1(H) &= 0, \end{aligned} \tag{A20}$$

a free-slip condition at the top of the domain is given by

$$\begin{aligned} v_z^1(H) &= 0 \\ \sigma_{xz}^1(H) &= 0, \end{aligned} \tag{A21}$$

and a free-surface upper boundary condition is

$$\begin{aligned} \sigma_{xz}^1(H) &= 0 \\ \sigma_{zz}^1(H) &= -\rho_1 g A_{\mathrm{surf}}, \end{aligned} \tag{A22}$$

where A_{surf} denotes the amplitude of the perturbation at the free surface and it is assumed that the density of air is negligible compared to the density of rocks.

Finally, we consider a fast erosion (or fast redistribution) upper boundary condition, which is essentially a free-surface boundary that is always maintained flat. The equations for this boundary condition are given by:

$$\begin{aligned} \sigma_{zz}^1(H) &= 0 \\ \sigma_{xz}^1(H) &= 0. \end{aligned} \tag{A23}$$

The resulting equations can be written in matrix form as (Ricard & Froidevaux 1986; Bassi & Bonnin 1988)

$$M\mathbf{C} = \mathbf{R}, \tag{A24}$$

where M is an 8×8 matrix, $\mathbf{C}$ an 8×1 vector containing the unknown coefficients and $\mathbf{R}$ an 8×1 vector containing density terms. If A_i indicates the amplitude of the sinusoidal perturbation of the ith interface (three in the current case), and $\mathbf{A}$ is a 3×1 vector containing A_i, $\mathbf{R}$ is given by

$$\mathbf{R} = P\mathbf{A}, \tag{A25}$$

where P is a 8×3 matrix containing forces due to density difference and gravity. The derivative of $\mathbf{A}$ versus time is given by

$$\frac{\partial \mathbf{A}}{\partial t} = \mathbf{V}, \tag{A26}$$

where $\mathbf{V}$ is a 3×1 vector containing the velocity at the ith interface. This velocity can be computed from the coefficient matrix $\mathbf{C}$ as (Bassi & Bonnin 1988)

$$\mathbf{V} = Q\mathbf{C} = QM^{-1}\mathbf{R} = QM^{-1}P\mathbf{A}, \tag{A27}$$

where Q is a 3×8 matrix containing coefficients required to compute velocity. An implicit time derivative of eq. (A26), yields

$$\frac{\mathbf{A} - \mathbf{A}^{\mathrm{old}}}{\Delta t} = QM^{-1}P\mathbf{A} = Q\mathbf{C}, \tag{A28}$$

which can be written as

$$\mathbf{A} = \mathbf{A}^{\mathrm{old}} + \Delta t Q\mathbf{C}, \tag{A29}$$

where $\mathbf{A}^{\mathrm{old}}$ denotes the amplitude at the old time step and Δt is the time step. Substituting eqs (A29) into (A25) and (A24) yields

$$(M - PQ\Delta t)\mathbf{C} = P\mathbf{A}^{\mathrm{old}}. \tag{A30}$$

Solving eq. (A30) for $\mathbf{C}$ allows to compute new amplitudes $\mathbf{A}$ according to eq. (A29). Practically we have implemented the governing equations in a MATLAB routine, which allows to compute the solution for an arbitrary number of layers (the approach is similar to the one described here except that there are $4 + 4n$ equations where n is the number of internal interfaces). In the case of a two-layer system with free-slip, no-slip or fast erosion upper boundary conditions, it is possible to compute the solution analytically. In this case we have used MAPLE scripts similar to the ones presented in Kaus (2005). The derived solutions have been used to verify the numerical code for purely viscous rheologies.